LEGIBILITY NOTICE

A major purpose of the Technical Information Center is to provide the broadest dissemination possible of information contained in DOE's Research and Development Reports to business, industry, the academic community, and federal, state and local governments.

Although a small portion of this report is not reproducible, it is being made available to expedite the availability of information on the research discussed herein.

ORNL/TM--10168

DE87 002074

An Algorithm for Unfolding Neutron Dose and Dose Equivalent from Digitized Recoil-Particle Tracks

Wesley E. Bolch
Department of Environmental Engineering Sciences
University of Florida
Gainesville, Florida 32611

and

J. E. Turner and R. N. Hamm
Health and Safety Research Division
Oak Ridge National Laboratory
Oak Ridge, Tennessee 37831

Date Published - October 1986

OAK RIDGE NATIONAL LABORATORY
Oak Ridge, Tennessee 37831
Operated by
MARTIN MARIETTA ENERGY SYSTEMS, INC.
for the
U.S. Department of Energy
Under Contract No. DE-AC05-84OR21400

TABLE OF CONTENTS

ACKNOWLEDGEMENT

The research of Wesley E. Bolch was performed under appointment to the Nuclear Engineering, Health Physics, and Radioactive Waste Management Fellowships Program administered by Oak Ridge Associated Universities for the U.S. Department of Energy.

An Algorithm for Unfolding Neutron Dose and Dose Equivalent from Digitized Recoil-Particle Tracks

Wesley E. Bolch, J. E. Turner and R. N. Hamm

Abstract

Previous work conducted at the Oak Ridge National Laboratory (ORNL) has demonstrated the feasibility of a digital approach to neutron dosimetry. In contrast to current analog methods, the digital approach specifically refers to methods of collection and processing of ionization products created by recoil particles within detector volumes. A dosimeter utilizing the digital approach would consist of both a detector and a computer algorithm. The detector would measure the integral number of subexcitation electrons produced by recoil particles within various subvolumes of its sensitive volume. The computer algorithm would unfold the quantities absorbed dose, linear energy transfer, and dose equivalent given that digital track-structure information.

ORNL researchers have completed a Monte Carlo simulation code of one detector design utilizing the operating principles of time-projection chambers. This thesis presents and verifies one version of the dosimeter's

computer algorithm. This algorithm processes the output of the ORNL simulation code, but is applicable to all detectors capable of digitizing recoil-particle tracks. Key features include direct measurement of track lengths and indentification of particle type for each registered event. The resulting dosimeter should allow more accurate determinations of neutron dose and dose equivalent compared with conventional dosimeters, which cannot measure these quantities directly. Verification of the algorithm was accomplished by running a variety of recoil particles through the simulated detector volume and comparing the resulting absorbed dose and dose equivalent to those unfolded by the algorithm.

CHAPTER 1

INTRODUCTION

In 1984, researchers at the Oak Ridge National Laboratory (ORNL) began work to design and construct an ionization chamber for neutron dosimetry based upon an entirely new concept for making digital measurements of charged-particle recoil tracks (Tu84,Tu85a). Current methods of dosimetry rely on the analog response of detectors to provide the information required to satisfy radiation-protection criteria. As documented in the next section, the existing methods suffer from a number of serious deficiencies. If successful, the new digital approach would be free of the restrictions inherent to analog techniques and would provide the most information one can obtain from ionization measurements. In the initial phase of the work at ORNL, a Monte Carlo computer code was written to simulate the expected digital response of a specific prototype design.

The objective of this thesis was to develop an algorithm which would unfold neutron absorbed dose, linear energy transfer (LET), and dose equivalent from the response of the design chamber. Assessment of the algorithm consisted of simulating detector responses to a variety of recoil tracks, and comparing the algorithm's unfolded values for average

absorbed dose, LET, and dose equivalent to those values calculated by the Monte Carlo code.

Need for Improved Neutron Dosimetry

The neutron dose equivalent received by a radiation worker is frequently measured by personnel dosimeters worn by that individual. Performance evaluations of such devices can be found in two reviews of Personnel Dosimetry Intercomparison Studies (PDIS) conducted from 1974 to 1983 at ORNL's Dosimetry Applications Research (DOSAR) facility (Si82,Si85). The majority of the personnel neutron dosimeters used in these intercomparisons were of five types: thermoluminescent albedo (TLD albedo) dosimeters, nuclear emulsion films, etched track detectors, TLD detectors, and combination detectors. The percentage of measurements made in the PDIS of each type were 48%, 18%, 15%, 13%, and 6%, respectively.

TLD dosimeters detect neutrons via the $^{6}Li(n,\alpha)^{3}H$ reaction in crystals of lithium fluoride. In addition, the $^{10}B(n,\alpha)^{7}Li$ reaction can be used within a chip of lithium borate. The response of an adjacent ^{7}LiF or $^{7}Li^{11}BO$ chip, both sensitive to gamma radiation only, is subtracted from the ^{6}LiF response to obtain neutron dose separately. These dosimeters can be responsive over a wide range of neutron energies.

TLD albedo dosimeters detect neutrons which are thermalized in and then reflected from the body. Incident thermal neutrons are shielded with boron or cadmium.

Etched track detectors use materials such as cellulose nitrate or polycarbonates in which recoil protons or carbon and oxygen ions are produced. Resulting damage tracks are made visible through subsequent electrochemical etching. Other designs incorporate foils of fissionable material for detection of incident thermal neutrons.

Combination detectors consist of both a TLD albedo detector, giving a low-energy response, and an adjacent etched track detector, giving a high-energy response. The combination provides more information to determine neutron dose than provided by either individually.

Nuclear emulsion films consist of a dispersion of silver halide within a layer of gelatinous material where incident neutrons undergo elastic scattering with hydrogen. Resulting proton tracks are enhanced by chemical reduction to grains of metallic silver so that they can be counted optically.

In the latter review (Si85), measurements from nine PDIS were compared to reference dosimetry values and the results categorized according to Nuclear Regulatory Commission (NRC) guidelines for +/- 30% precision and +/- 50% accuracy. The authors found that precision was not a problem in personnel neutron dosimetry in that over 90% of all dosimeters tested met this criterion. Film dosimeters gave the poorest results with 78% meeting the criterion. The accuracy criterion, however, was not being met in that only 60% of all measurements were within 50% of the reference value. The combination detectors were the most accurate with 77%

meeting the criterion, followed by the TLD albedo with 70% meeting the criterion. Film dosimeters were the least accurate with only 29% meeting the accuracy criterion. The authors point out that all measurements were made under ideal conditions.

Another technique used to assess personnel neutron dose in radiation areas is to measure dose rates with area or survey monitoring devices and record the time individuals remain in those areas. These devices are additionally used to calibrate personnel neutron dosimeters in unknown fields (Pi85). One indirect method of determining neutron dose equivalent with survey meters involves measuring the neutron fluence rate as a function of energy and applying an energy-dependent conversion factor giving dose equivalent per unit fluence. The neutron energy spectrum is obtained by applying unfolding techniques to the response of fast neutron detectors which utilize either the $^{6}Li(n,\alpha)$ reaction, the $^{3}He(n,p)$ reaction, or elastic scattering with hydrogen (Kn79). The conversion factors are frequently obtained from Monte Carlo simulations of monoenergetic neutrons incident upon cylinders or spheres of tissue equivalent material (Cr85,ICRP71,NCRP71).

There are several problems with the use of fluence-to-dose conversion factors (In85). First, the factors differ depending upon the shape and composition of the phantom used in the simulation; quoted values of dose equivalent are thus "virtually meaningless" unless the particular simulation

parameters used to compute dose equivalent are given (Ro79). Second, conversion factors were calculated from the maxima of the generated dose distribution curves in order to give a conservative estimate of the dose equivalent. The depth at which these maxima occur, however, vary with the energy of the incident neutron such that calculation of neutron dose equivalent in fields with a distribution of neutron energies becomes arbitrary. Third, the two most commonly used tabulations of conversion factors, given in the National Council on Radiation Protection and Measurements (NCRP) Report 38 and the International Commission on Radiological Protection (ICRP) Report 21, differ by as much as a factor of two due to different interpolation schemes. Recent calculations by Cross and Ing support those of ICRP Report 21 (Cr85).

A second method of indirectly determining neutron dose equivalent with survey or area monitors is to use moderator-type devices. These instruments consist of spheres or cylinders of polyethylene surrounding a thermal neutron detector such as a ^{6}LiF TLD or a ^{3}He proportional counter. Incident neutrons are thermalized via elastic collisions in the polyethylene where a certain fraction reach the embedded detector. These dosimeters can be designed so that their energy response is matched to one of the dose equivalent conversion-factor curves mentioned above.

These devices, however, produce reliable measurements only if great care is used in interpreting their response. One author reports that the response of a moderator dosimeter is highly sensitive to the directional characteristics

of the neutron field. The author additionally states that if the instrument is calibrated in a monodirectional field, then there can be an overresponse by a factor of three or four if the device is used in an isotropic field such as occurs around many reactors (Ro79). In one situation, the author found the dosimeter overresponding by a factor of 15. Even if the directional response of the moderator dosimeter is taken into account, the uncertainties inherent in the conversion factors they attempt to match still persist.

Considering the unsatisfactory performance of personnel neutron dosimeters, survey meters, and area monitors, recent instrumentation design efforts have emphasized the direct measurement of neutron dose equivalent. In the following sections, current dosimeter techniques employing analog methods of charge collection to infer dose equivalent will be discussed. This will provide a comparative basis for introducing the advantages of ORNL's proposed digital technique of charge collection to infer that same quantity. First, however, a review of the formal definition of the dose equivalent as it applies to neutron dosimetry is needed.

Neutron Dose Equivalent

Neutrons are particles which cause ionization in matter indirectly via production of energetic charged nuclear-recoil particles. These charged recoil nuclei result from either elastic collisions, inelastic collisions, or nuclear reactions between the incident neutrons and the atoms

constituting the target matter. When neutrons irradiate tissue, the energy transferred to target cells by these secondary charged-particles can produce damaging biological effects. The unit of dose equivalent measures not only the density of this energy deposition per unit tissue mass, but the relative effectiveness of that energy deposition for producing biological damage. This relative effectiveness is dependent upon the type and energy of the particle which deposited the energy.

Energy deposited per unit mass is referred to as absorbed dose, D, while the relative effectiveness of different particle types and energies for producing biological damage is quantitated by a weighting factor, Q, referred to as the quality factor. The dose equivalent, H, is defined as the product of D and Q. Conventional neutron dosimeters are only able to measure D, giving either its total integral value, or D as a function of neutron energy. To calculate H, one must use either a single Q averaged over all neutron energies or average Q's given as a function of neutron energy (NCRP71). A dosimeter which claims to measure H directly, however, must measure D and Q directly in a manner dependent upon their formal definitions.

Absorbed dose, D, is formally defined as the quotient of $d\bar{\varepsilon}$ by dm, where $d\bar{\varepsilon}$ is the mean energy imparted by ionizing radiation to matter in a volume element of mass dm (ICRU77). Absorbed dose in an irradiated target is regarded as a function, having a value at every point in that target.

It is, in this respect, "something of a theoretical abstraction" which cannot be measured (Gr85). When an ionization detector collects charges produced from the passage of a charged particle, the quantity actually measured is the microdosimetric quantity, specific energy. Specific energy, z, is defined as the quotient of ε by m, where ε is the energy imparted during the event to a volume of mass m (ICRU77). Over a given irradiation interval, measured values of the stochastic quantity z will form a distribution from which a non-stochastic mean specific energy, $\bar{z}$, can be obtained. Greening (Gr85) relates absorbed dose D to the mean specific energy by the expression

$$D = \lim_{m \to \emptyset} \bar{z}. \qquad (1)$$

For neutrons, one can disregard the limiting procedure provided that the fluences of neutrons and their secondaries are uniform throughout the sensitive volume, and that the corresponding measurement of D is large (ICRU77). Thus by measuring the mean specific energy, $\bar{z}$, one can report an absorbed dose, D.

The measurement of specific energies is usually accomplished under two assumptions. First, the mean energy expended in the production of an ion pair (W-value) in the counter gas is known and is independent of the type and energy of all initiating particles. Second, the ionization products are collected in such a manner that the height of the resulting electrical pulse is directly proportional to

the number collected, a condition realized in a proportional counter.

Absorbed dose accounts for the total amount of energy deposition in tissue; however, yields of radiochemical products thought to produce biological damage are also dependent upon the spatial distribution of this energy deposition. The macrodosimetric quantity LET, or linear energy transfer, was thus defined in an attempt to account for the microscopic distribution of the energy deposited by charged particles. The restricted LET, LET_{Δ}, of a charged particle in matter is defined as the quotient of dE by dl, where dE is the energy loss due to electronic collisions with energy transfers less than some specified value Δ, and dl is the distance traversed:

$$L_{\Delta} = (dE/dl)_{\Delta}. \qquad (2)$$

Restricted LET attempts to account for energy deposited "locally" within a small volume of matter, contrasted to the energy lost by the charged particle in that same volume. LET_{Δ} reflects the fact that some of the transferred energy may be carried out of the volume by energetic secondary electrons produced during ionization. If the volume of interest is sufficiently large so as to absorb all the energy lost by the charged particle, the particle's LET equals its unrestricted linear energy transfer, LET_{∞}.

To evaluate dose equivalent, absorbed dose is weighted by a quality factor, Q, to account for these energy distribution effects, where Q is currently defined in ICRP Report 26

(ICRP77) for specific values of L_∞ in water (see Table 1). Secondary charged particles produced in tissue by neutrons of various energies exhibit a wide range of LET values; NCRP Report 38 (NCRP71), therefore, has previously extended these point definitions of Q through interpolation to obtain LET intervals over which a particular value of Q is to be used (see Table 2). These interval definitions give a step-function approximation to the continuous curve of quality factor versus LET given in ICRP Report 26 and as shown in Figure 1.

When ionizing particles deliver absorbed dose over a range of LET values, dose equivalent is given as

$$H = \int_{L_{min}}^{L_{max}} D(L)Q(L)\, dL, \qquad (3)$$

where D(L) is the absorbed dose delivered by all particles with LET L, and Q(L) is the quality factor at L (NCRP71). Conventional dosimetry is unable to provide D(L) and, therefore, dose equivalent is determined by using the average quality factors mentioned at the beginning of this section. Recent advances in microelectronics, however, have allowed us to measure D(L) in real-time and thus return to the more formal definition given above.

Direct Determination of H by Analog Charge Collection

Conventionally, D(L) has been obtained only through a knowledge of the distributions of absorbed dose and LET within the sensitive volume of a detector. The absorbed dose distributions are obtained directly from acquired pulse-

TABLE 1
Quality Factor Q versus Unrestricted LET in Water (keV/μm)
from ICRP Report 26 (ICRP77)

L (keV/μm)	Q
3.5 (and less)	1
7	2
23	5
53	10
175 (and above)	20

TABLE 2
Quality Factor Q for specified intervals of LET
from NCRP Report 38 (NCRP71)

L (keV/μm)	Q
3.5 (and less)	1.00
3.5 - 7.0	1.50
7.0 - 15.0	2.82
15.0 - 25.0	4.47
25.0 - 35.0	6.18
35.0 - 50.0	8.28
50.0 - 62.5	10.30
62.5 - 75.0	11.80
75.0 - 87.5	13.60
87.5 - 100.0	14.90
100.0 - 200.0	17.50
200.0 (and above)	20.00

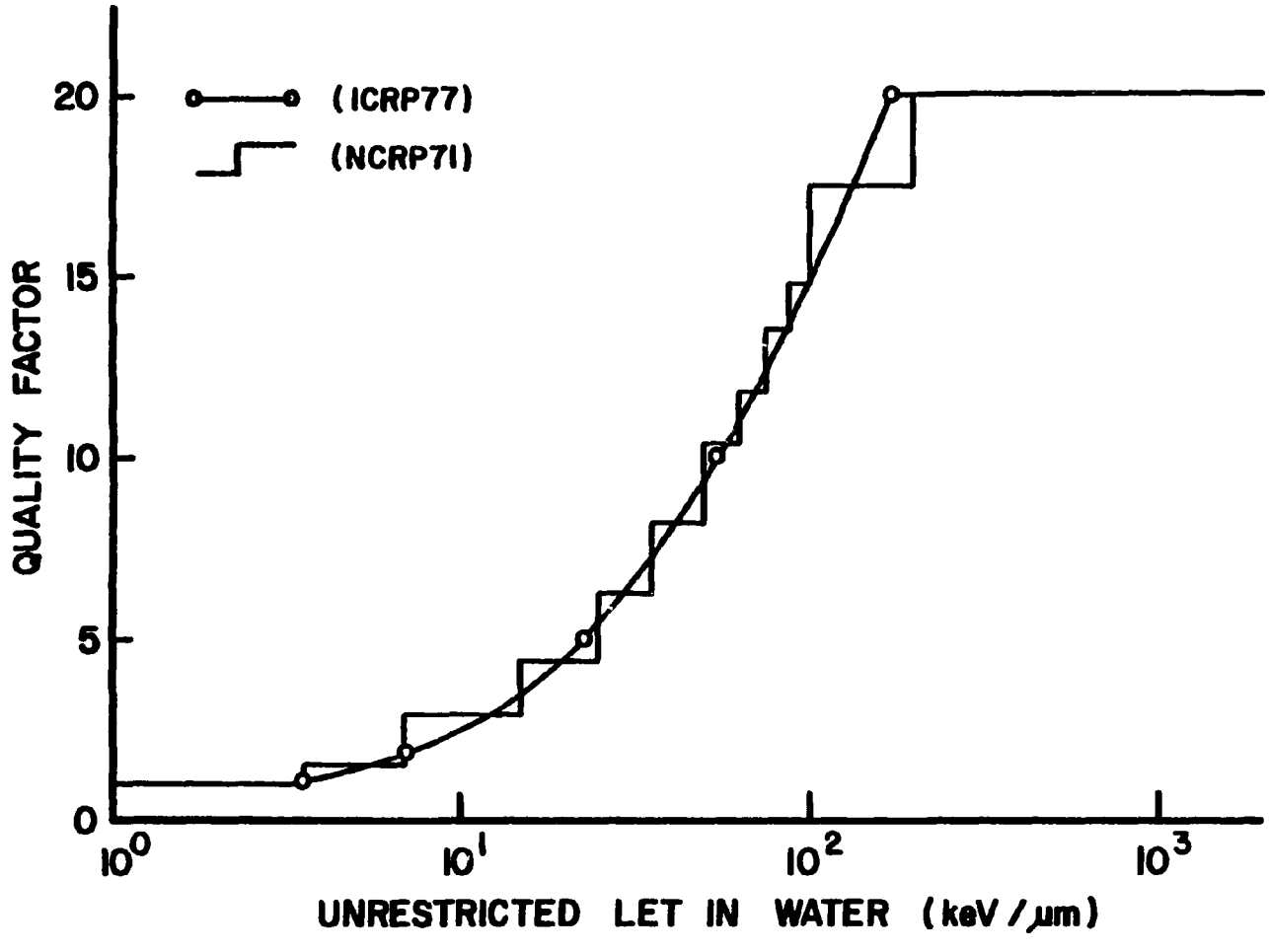

Figure 1. Quality factor versus unrestricted LET in water.

height spectra assuming all collected pulses are directly proportional to the energy deposited by events in the sensitive volume. The LET distributions are obtained through computer unfolding routines applied to the pulse height spectra.

One technique of unfolding LET spectra from pulse-height spectra was investigated by the ORNL group prior to the development of plans for the digital approach (To82). The technique uses a Hurst proportional counter to obtain a pulse-height spectrum upon irradiation in a neutron field. The detector is constructed of polyethylene walls with cyclopropane fill gas. Most of the events produced are recoil protons which completely traverse the chamber. Energy deposited by the recoils is assumed to be equal to the product of their track length in the sensitive volume and their average LET. A distribution of recoil-proton track lengths for isotropic chords traversing the sensitive volume is computed and stored. The unfolding technique begins by initially assuming that the protons have a flat LET distribution in the chamber. The track-length and LET distributions are then randomly sampled and their values multiplied in pairs to produce a trial pulse-height spectrum. Residuals between the measured and trial pulse-height spectra are then used to readjust the assumed LET spectrum. This iteration process of adjusting the LET spectrum is repeated until the calculated pulse-height spectrum matches the observed spectrum. Convergence of the pulse-height spectrum and stabilization of the LET spectrum occur after

approximately 10 iterations of 10,000 samplings each.

Unfolding techniques like that given above unfortunately cannot give the health physicist a real-time assessment of dose equivalent in neutron fields. As mentioned in the last section, microprocesso can now be integrated into detector designs so that individual pulses can be processed by algorithms as soon as they are collected. One dosimeter type which exhibits these properties is the current version of the tissue equivalent proportional counter (TEPC). This device has been used for a number of years as a laboratory instrument, but recently has seen some use as an operational health physics dosimeter (Br85). TEPC detectors are hollow spheres of tissue-equivalent plastic filled with tissue-equivalent gas. Low gas pressures are used so as to simulate spherical tissue volumes of one to five μm, and also allow recoil secondaries generated from the walls to completely cross the cavity volume. The TEPC utilizes microdosimetric principles to infer energy deposition and LET for each registered event.

As stated earlier, absorbed dose is estimated by measuring the mean specific energy, $\bar{z}$. The best estimate of $\bar{z}$ is the total energy imparted by all events i, i running from one to n registered events, divided by the mass of the sensitive volume, m (Ng85).

$$D = \frac{1}{m} \Sigma_i \varepsilon_i. \qquad (4)$$

For each registered event, electrons produced by ionization

are collected at a central electrode producing an electrical pulse. Under the assumption of a constant W-value in the counting gas for all secondaries produced and linear amplification of each pulse collected, the energy imparted by each event i is equal to the product of the measured pulse height h_i and a calibration constant c. Absorbed dose is thus given as

$$D = \frac{c}{m} \Sigma_i h_i. \qquad (5)$$

In neutron dosimetry, the W-value for a specific event can vary with the type and energy of secondary particle produced (Gr85). These variations with secondary type and energy complicate the process of determining an average W-value since changes in incident neutron energy produce corresponding changes in the relative abundance and average energies of the secondary particles they produce. Additionally, W-values change with gas type; therefore, once an average is obtained for a specific gas type, one must further average W-values over the complex mixture of gases used to produce a tissue-equivalent counting gas. With all uncertainties considered, a typical W-value for all secondaries produced by neutrons with energies between 1 and 20 MeV within tissue equivalent gas is thought to be 31.3 eV/ion pair (Gr85).

The next piece of information needed by the TEPC is the average LET experienced by the particle, which can be inferred from measurements of its microdosimetric equivalent, lineal energy (Ng85). Lineal energy, y, is defined as the

quotient of ε by d where ε is the energy imparted by an event within a detector's sensitive volume and d is chord length traversed by the charged particle within that volume (ICRU77). Except for pulse rise-time, the TEPC has no information concerning the chord length traced by individual events. The mean chord length, $\bar{d}$, for isotropically incident particles is therefore substituted in the expression for lineal energy. For convex bodies, $\bar{d}$ is equal to 4V/S, where V is the volume and S is the surface area of the detector cavity. For spherical bodies such as the TEPC, $\bar{d}$ becomes 2d/3, where d is the diameter of the sphere.

No standard relationship exists between linear energy transfer, L, and lineal energy, y. The TEPC relies upon an approximation given by Rossi which is valid under three conditions (Ng85). First, the sensitive volume must be small enough such that L does not change appreciably during the traversal of the particle. Second, particles must completely traverse the volume in straight lines. Third, energy deposition must be localized within the sensitive volume. Provided these assumptions are met by the TEPC, Nguyen relates average LET to average lineal energy by

$$\bar{L} = \frac{8}{9}\bar{y}. \qquad (6)$$

By approximating each event by its average and incorporating the definition of the mean chord length in a sphere, the above relation gives the LET of event i as

$$L_i = \frac{4}{3} \frac{c}{d} h_i. \qquad (7)$$

The LET of event i, L_i , can therefore be used to find the appropriate quality factor, $Q(L_i)$, associated with that event.

Using the quality factors defined over intervals of LET as given in Table 2, Equation 3 shows that to determine dose equivalent, H, one must determine the total absorbed dose, D(L), in each LET interval, L, multiply each D(L) by the appropriate quality factor, Q(L), for that interval, and sum over all LET intervals.

$$H = \Sigma_L \, D(L)Q(L) = \Sigma_L \, H(L). \qquad (8)$$

Utilizing Equation 5 for approximating D(L) and folding in the appropriate quality factor, Q(L), the dose equivalent, H(L), delivered by events within LET interval L is given as

$$H(L) = \frac{c}{m} \Sigma_i \, h_i(L)Q(L), \qquad (9)$$

where i runs over all events with inferred LET in interval L. Total dose equivalent then becomes

$$H = \frac{c}{m} \Sigma_L \, \Sigma_i \, h_i(L)Q(L). \qquad (10)$$

Since each event is processed as it occurs randomly in nature, the order of the above summations becomes meaningless. Neutron dose equivalent is therefore measured by the TEPC through the operational equation

$$H = \frac{c}{m} \Sigma_i h_i Q(L_i). \qquad (11)$$

In two reviews of the TEPC, the dosimeter was found to give "reasonable" values for neutron dose equivalent at neutron energies between 100 keV and 14 MeV (Ng85,Br85). In all cases, however, dose equivalent was found to be underestimated; such underresponses reached 40% at energies 200 keV and 5 MeV. Nevertheless, Brackenbush claims that accuracy, sensitivity, and lower limits of detection are "acceptable" for personnel dosimetry. Gamma events are identified through pulse-height discrimination, yet this feature contributes to underestimates of dose equivalent at neutron energies below 10 keV where $H(n,\gamma)D$ reactions are important.

Nguyen sites that optimum gas pressures depend upon compromises between signal-to-noise considerations at low pressures versus stopper/starter effects at higher pressures. Starters are recoils created within the gas volume, while stoppers are recoils which do not completely traverse the volume before losing all their kinetic energy. Since the requirement for complete cavity traversal is violated for both starters and stoppers, LET approximations by Equation 6 become invalid for these events which become more frequent with increasing gas pressure.

Direct Determination of H by Digital Charge Collection

Direct measurements of neutron dose equivalent by the TEPC are limited primarily through uncertainties in inferences of energy deposition and LET for each event

detected. Provided the device is electronically calibrated, the major uncertainty in the energy imparted by an event is in the assumption of a constant W-value for all secondary particle types and energies seen by the detector. The major uncertainty in the LET for each event is in the validity of Equation 6 on an event-by-event basis. Additionally, since Equation 6 uses lineal energy (as defined by the quotient of energy deposition and average chord length) to infer LET, uncertainties in LET are coupled to uncertainties in energy deposition as well as actual track-length distributions in the sensitive volume. The validity of TEPC measurements, therefore, is dependent not upon correctly measuring these quantities for each event, but upon being correct on the average for many events.

A dosimeter which would determine energy deposition and track length correctly for each registered event would prove more versatile than the TEPC and would, in theory, more accurately unfold neutron dose equivalent. Such a dosimeter would include both a detector to collect all physical data needed to determine energy deposition and track length for each event, and an algorithm to unfold those quantities from the data provided.

In designing the detector portion of the dosimeter, one can ask: What is the most information physically available to characterize the passage of a charged particle through a gas? For an ionization chamber, the spatial coordinates of every primary and secondary electron produced by that parti-

cle represent the total "information" the particle transfers to the detector. In conventional chambers, this charge is collected in such a fashion that spatial information is either not available or is only indirectly available (e.g., such as using measured pulse rise-time to infer the spatial extent of an ionization track). The new concept of a digital dosimeter will attempt to utilize modern measurement techniques, similar to those of the time-projection chamber in elementary-particle physics, to measure the spatial coordinates of these electrons.

The algorithm portion of the dosimeter, which is the subject of this thesis, furnishes the means for determining track length and energy deposition for each event given this digital information. Since the algorithm's input data essentially give a three-dimensional "picture" of the event, the track length in the sensitive volume is obtained by locating its endpoints to within the accuracy of the detector's spatial resolution. Unlike the TEPC, energy deposition is obtained by first identifying the secondary-particle type (e.g., recoil proton or carbon ion). Identification is accomplished by inferring an average specific ionization (ion pairs per unit track length), a quantity which is unique to particle type over the energy ranges encountered by the detector. Curves of W-value as a function of energy for each particle type and each component of the counting-gas mixture are available to the algorithm; therefore, once the particle type is known, the algorithm can use these curves to more accurately obtain energy deposited by the

event. With both track length and energy deposition unfolded, the algorithm calculates an average LET, obtains a quality factor for the event from values given in Table 2, and calculates the event's contribution to the total dose equivalent.

In addition to measuring the dose and dose equivalent for each individual event, the digital dosimeter offers additional advantages over the TEPC. First, the digital method does not depend upon all tracks completely crossing the sensitive volume. Stoppers, starters, and inners (particles that both start and stop within the sensitive volume) can be analyzed, thus presenting no restrictions upon gas pressure. Optimal pressures would depend, among other things, on the spatial resolution needed for resolving low-energy inners. Second, in addition to pulse-height discrimination of gamma events, track-structure information such as specific ionization would lead to easy identification of Compton electrons and photoelectrons. Third, whereas coincident events are registered as single events in the TEPC, a digital algorithm could, in principle, analyze two or more events coincident in time, but not in space.

Other Applications of Digital Dosimetry

A "hierarchy of designs" for a dosimeter based upon digital charge collection can be considered (Tu84,Tu85a). As inferred within the previous section, an ultimate design of the detector would resolve single electrons, thus providing a research instrument for the field of microdosimetry.

With exact track-structure information, one could use such a device in microdosimetry experiments to better correlate free radical formation with damage sites found within organic molecules adjacent to particle tracks. As design spatial resolution decreases, electron coordinates would be known only within the dimensions of subvolumes within the detector. These subvolumes, or "cells," would then function as independent detectors where partial energy deposition for each event would be registered. A particle track would be registered as a set of integers, giving the number of electrons initially occurring in each cell. With the passage of many tracks within the detector, distributions of specific energy and lineal energy can be tabulated for each cell, these distributions also important in microdosimetry.

As spatial resolution decreases further, one does not have information on differential track structure, but overall track length can still be obtained. This is the level of sophistication needed for neutron dosimetry as discussed above. As spatial resolution is further decreased, one is left with no track-structure information, as is the case with the TEPC and other conventional dosimeters.

CHAPTER 2

DESCRIPTION OF NEUTRON DETECTOR DESIGN

As stated in the previous chapter, ORNL's proposed neutron dosimeter based upon digital charge collection consists of a detector to collect charged-particle recoil-track information and an algorithm to use that information to infer neutron dose, LET, and dose equivalent. Since the algorithm is dependent upon, and is only as good as, the detector which provides its input, it is essential to understand the detector design upon which the algorithm is based. This chapter, therefore, will discuss the current detector design including its wall material, counting gas, and proposed method of obtaining digitization of recoil tracks. This design presents several physical limitations to track reconstruction and these will also be presented.

Detector Wall Material and Counting Gas

The operation of many radiation dosimeters is based upon the Bragg-Gray theory. This theory allows one to infer absorbed dose in a material by measuring the ionization within a gas-filled cavity inside that material. Since dose to human tissue is of fundamental concern in neutron dosimetry, the material used to construct the detector should be tissue equivalent, its atomic composition matching that of tissue. Neutron interactions in matter depend upon both atom type and number density; therefore, tissue equivalence

insures that all reactions which occur in tissue are simulated in type and frequency within the wall material.

Figure 2 shows tissue kerma per unit fluence for various neutron interactions as a function of neutron energy. Kerma, K, is defined as the quotient of dE_{tr} by dm, where dE_{tr} is the sum of the initial kinetic energies of all charged particles liberated by indirectly ionizing particles in a volume element of mass dm (ICRU77). Since the range of the majority of neutron-produced secondary particles in tissue is small, kerma gives a very good approximation to absorbed dose in neutron dosimetry. The figure shows that for neutron energies above 1 keV, tissue kerma is principally due to elastic scattering with hydrogen. Specifically, this mechanism contributes 97% of total kerma at 10 keV decreasing to 69% at 18 Mev. Matching the hydrogen content of tissue is therefore very important. The next three most important contributors to tissue kerma are elastic collisions with oxygen, carbon, and nitrogen. Since most tissue equivalent materials are made from hydrocarbons, the normal procedure has been to substitute carbon for oxygen and nitrogen. When elastic scattering is the principal interaction considered, this substitution introduces little error since the atomic number and charge of recoil oxygen and nitrogen ions are close to those of carbon ions.

Polyethylene was chosen for the wall material in the initial detector design. According to Report 26 of the International Commission on Radiation Units and Measurements (ICRU), the percent elemental weight for H and C in polyeth-

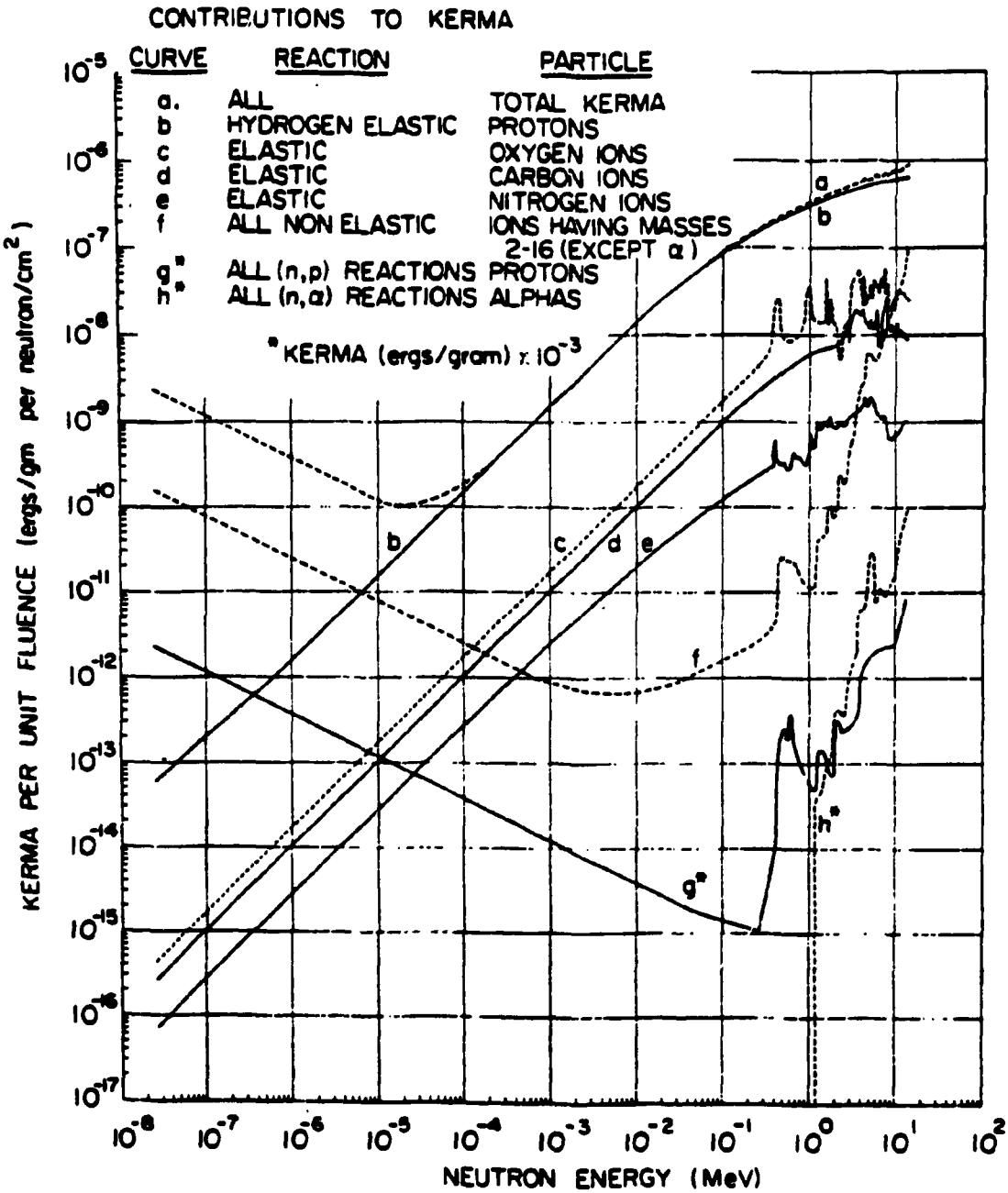

Figure 2. Tissue kerma per unit fluence as a function of neutron energy (NCRP71).

ylene are 14.4 and 85.6, respectively (ICRU77). Percentages for H, C, N, and O for tissue in standard man are 10.0, 18.0, 3.0, and 65.0%, where the total percentage of C, N, and O is 88.0%. The material thus matches tissue composition with the carbon substitution. The principal secondary events in simulation models of the chamber will therefore be recoil protons and carbon ions produced from elastic scattering.

The Bragg-Gray principle states that the ratio of absorbed dose in the wall material to absorbed dose in the gas cavity is equal to the corresponding ratio of the average mass stopping power of charged particles within in the wall material to their average mass stopping power within the gas cavity,

$$D_m / D_g = (S/\rho)_m / (S/\rho)_g = S_{mg}. \qquad (12)$$

(The stopping power, S, of a charged particle in a medium is equal to its unrestricted linear energy transfer).

This principle requires four conditions to be satisfied (Gr85). First, secondary charged particles must lose energy in a large number of very small energy loss events. Second, charged particle equilibrium must be established within the wall material. Third, the mass stopping power ratio, S_{mg}, must not vary significantly with the energy of the secondary particle. Fourth, the gas cavity must not disturb the charged particle fluence or its distribution in energy and direction emerging from the inside surface of the detector wall.

The first condition is physically satisfied for neutron-produced secondary charged-particles. Equilibrium of charged-particle fluence needed in the second condition is attained by making the wall thickness at least equal to the maximum range of all secondary particles produced. The proposed chamber is to be used for neutron energies up to 20 MeV. Since elastic scattering with hydrogen produces recoil particles with the greatest range, the detector's wall thickness should be equal to the range of a 20 MeV proton in polyethylene, that range being approximately 0.42 cm (NAS64).

One can satisfy the last two conditions by making the detector homogeneous such that the atomic composition of the fill gas matches that of the wall material. In such detectors, S_{mg} becomes unity and independent of secondary energy. In addition, the requirement for uniform fluence of secondaries through the cavity is achieved through applying a theorem by Fano. Fano's theorem states that given a uniform flux of neutrons, the flux of secondaries in a material is also uniform and is independent of the density of the medium (Gr85). Introduction of a low-density cavity into a medium, therefore, does not disturb secondary fluence provided the cavity material has the same elemental composition. In addition, Fano's theorem places no restrictions upon cavity size.

To construct a homogeneous chamber with polyethylene walls, the logical choice for a fill gas would be ethylene.

Methane was chosen for the initial design work, however, since the data on cross sections, W-values, electron diffusion, and stopping powers needed for the Monte Carlo transport code, as well as the algorithm itself, are better known for that gas. Elemental percentages of hydrogen and carbon for methane are 25.1% and 74.9%, respectively. This configuration is thus only approximately homogeneous, but is adequate for preliminary design studies. The design pressure of the methane counting gas was set at 10 torr in order to allow spatial resolution of carbon ions down to a few keV. The final chamber design specifies polyethylene walls at least 0.42 cm thick with methane fill gas at 10 torr.

Track Digitization by Proportional Counting

Initial designs for track digitization envisioned a detector with a sensitive volume as diagrammed in Figure 3 (Tu84). This volume is a cube with each edge 10 cm in length. The origin for a reference set of XYZ axes is located at one of its corners. The cross-hatched area at the bottom XY plane of the cube represents a 10 x 10 array of independently operated needle electrodes, each spaced 1 cm apart in the X and Y directions, and each operated within the proportional region of its operating curve. Reference to a particular electrode is made by specifying its (i,j) coordinates, i and j both running from 1 to 10 along the X and Y axes, respectively. Electrons produced by secondary track ionization are swept toward these electrodes under a constant potential, and are registered in this array of

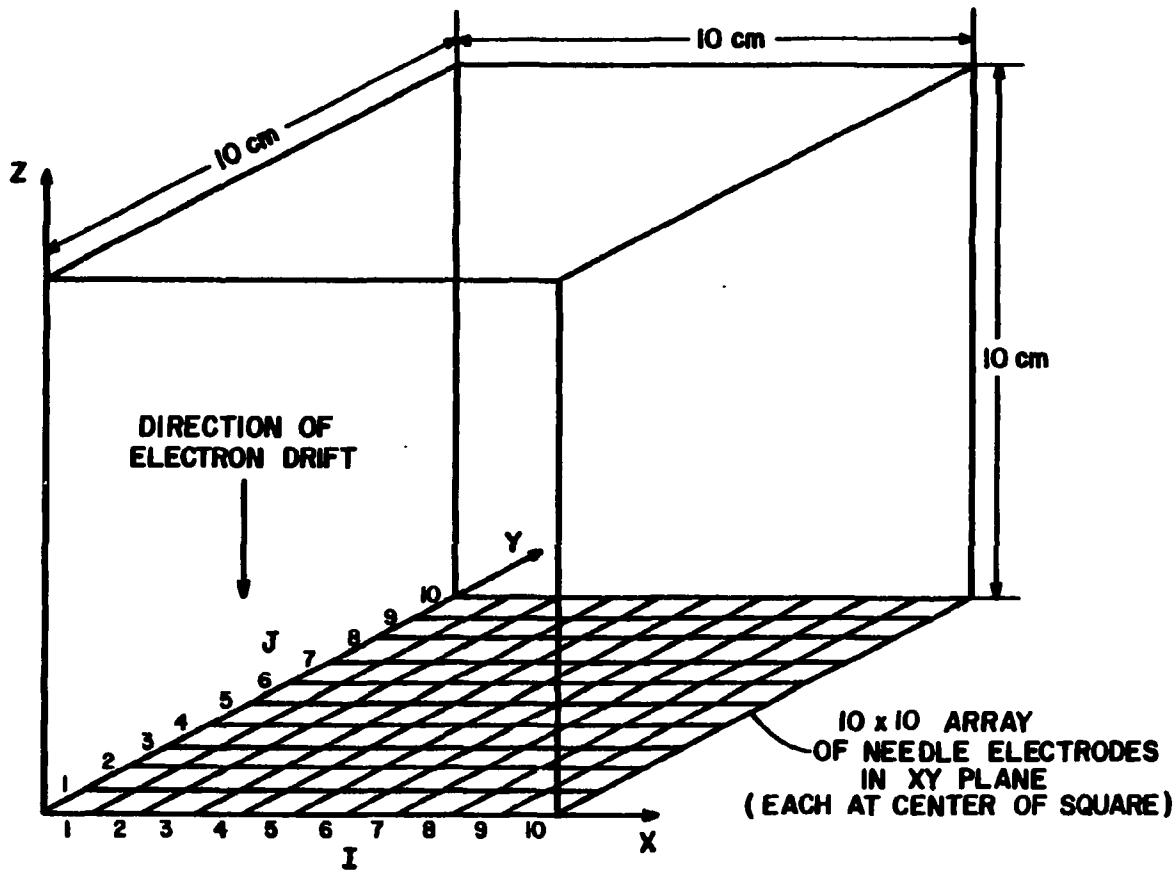

Figure 3. Sensitive volume of detector.

proportional counters inferring their spatial coordinates to within +/- 1 cm.

As with time-projection chambers, the relative Z coordinates of electrons are determined from measuring arrival times at the collecting electrodes. For a given gas pressure and electric field strength, the drift velocity for electrons can be calculated (Kn79). Charge collection at each electrode can be time-resolved to give a 1 cm resolution in the Z direction. In this manner, the sensitive volume is subdivided in the vertical into 10 virtual subvolumes located above each electrode. Each virtual subvolume is referenced by an index k, where in the case of 1 cm drift resolution, k runs from 1 to 10 in the positive Z direction.

The detector design chosen for developing a working algorithm therefore has a cubical sensitive volume, 10 cm on a side, which is effectively partitioned into a 10 x 10 x 10 array of 1 cm^3 detection subvolumes or "cells." All cells containing at least one electron are referred to as "triggered" cells. The simulated detector output thus produces 1000 (i,j,k) integers for each recoil track registered, each integer representing the number of electrons produced within the corresponding cell.

To demonstrate, Figure 4 shows the true three-dimensional coordinates of every subexcitation electron produced by a 500 keV recoil proton in the sensitive volume as calculated by the Monte Carlo simulation code. Figure 5 shows the two-dimensional projection of that track onto the

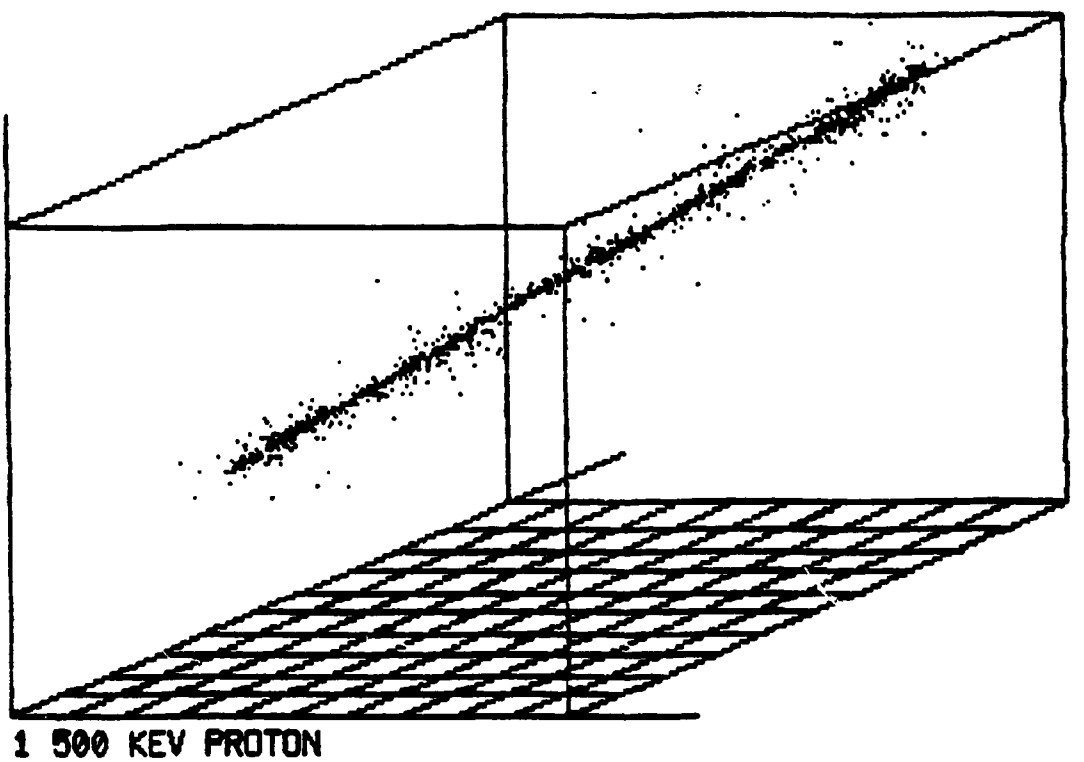

Figure 4. Simulated ionization track produced by a 5ØØ keV proton.

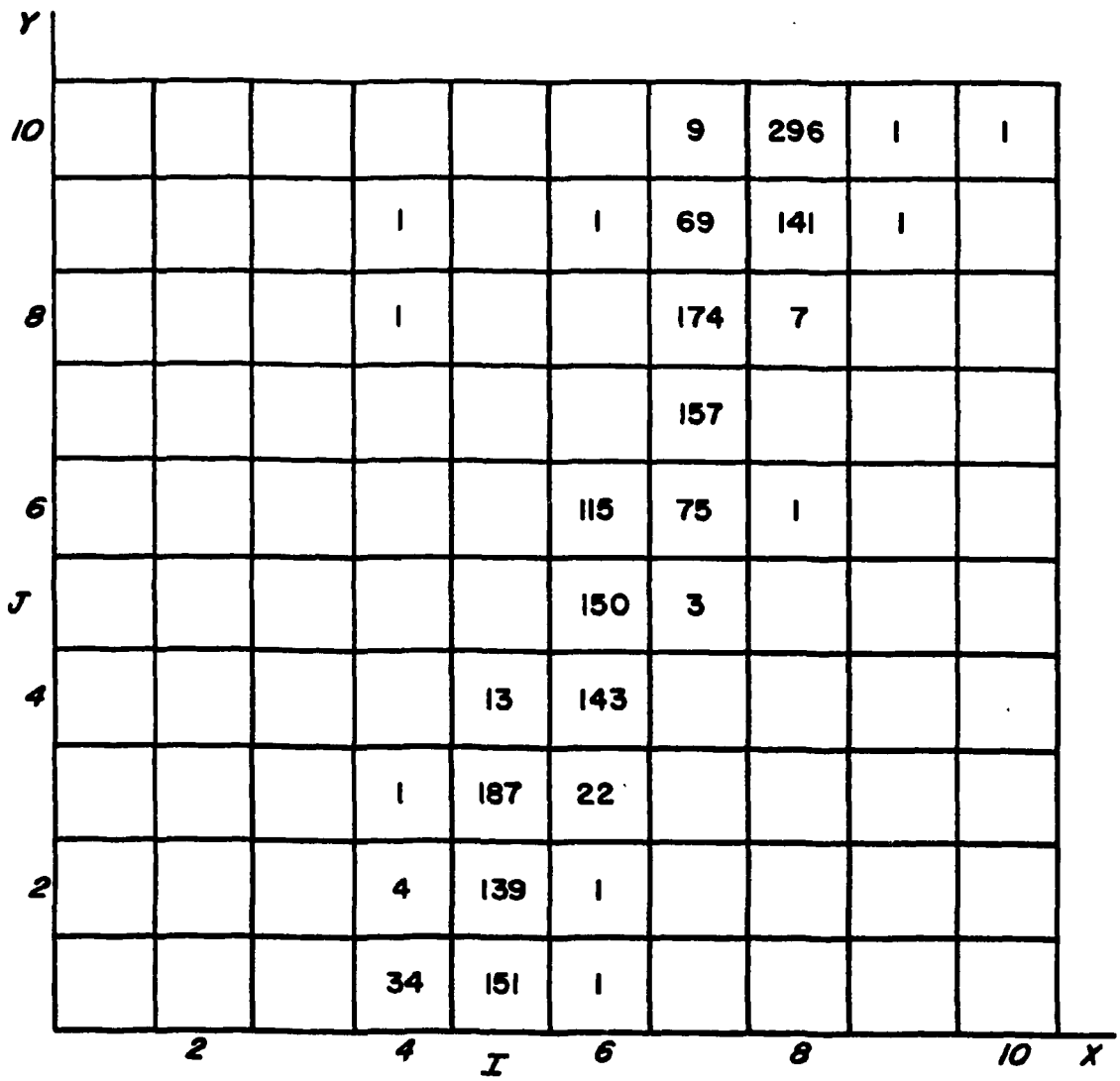

Figure 5. Numbers of electrons produced by the 5ØØ keV proton which are registered within the XY collection plane (neglecting thermal diffusion).

XY plane as reconstructed by the detector. The 100 integers appearing in Figure 5 represent the 1000 integer output array summed over all k, with zero collected electrons not indicated. Figures 6 and 7 show those same features for a 80 keV carbon recoil.

Physical Limitations to Track Reconstruction

When assessing the algorithm portion of the detector, one must keep in mind the physical limitations of the detector. These limitations can be attributed to either the collection electronics, or more fundamentally, to the physics of charged-particle energy deposition.

In the discussions which follow, recoil particles and the ionization tracks they produce will sometimes be referenced by one of four possible classes: stoppers, starters, inners, and crossers, names referring to the position and extent of the track in the sensitive volume. Stoppers are tracks produced by recoil particles emerging from the inside surface of the detector wall but which terminate within the sensitive volume. Starters are tracks which start within the sensitive volume from a neutron collision with a gas-molecule nuclei, and which terminate within the detector wall. Inners are similarly produced within the gas volume but also terminate within that volume. Crossers are tracks produced by recoils originating in the wall which are energetic enough to completely traverse the chamber cavity.

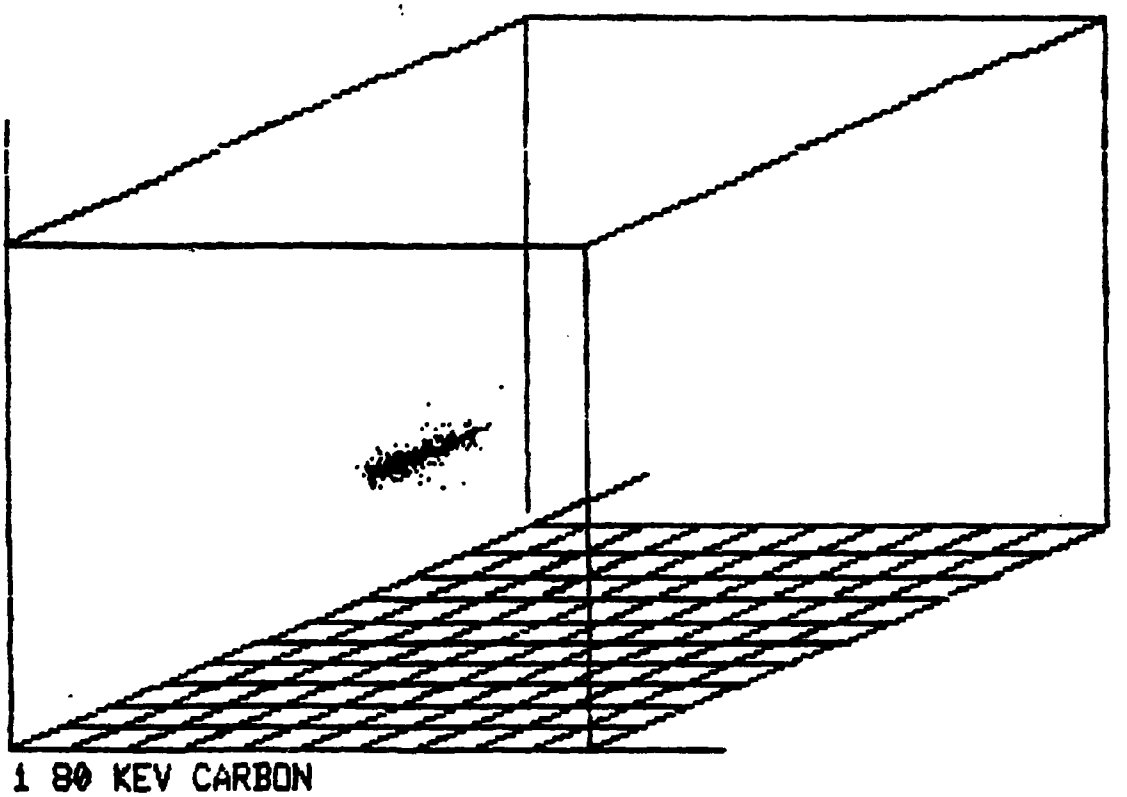

Figure 6. Simulated ionization track produced by an 80 keV carbon ion.

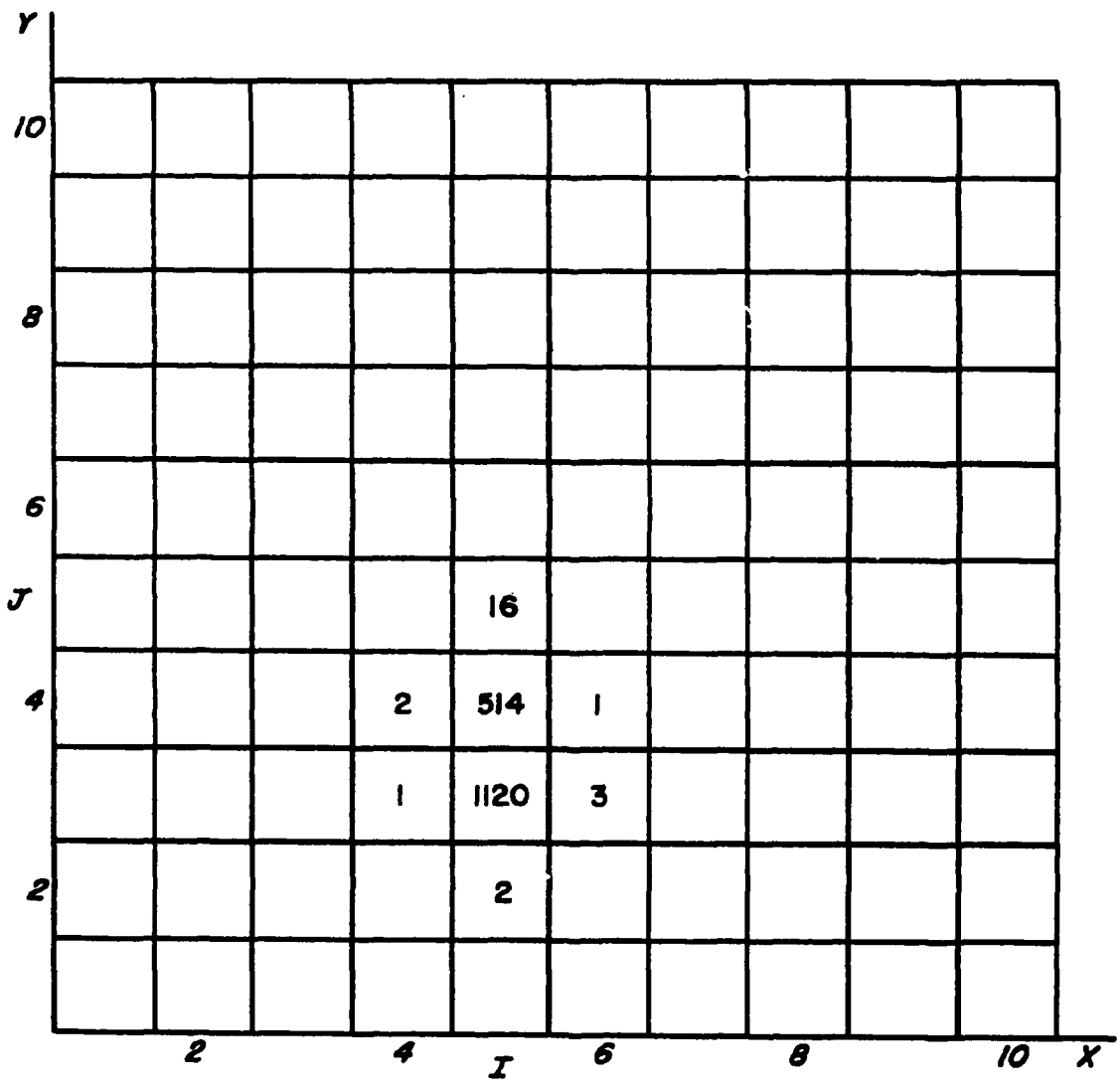

Figure 7. Numbers of electrons produced by the 80 keV carbon ion which are registered within the XY collection plane (neglecting thermal diffusion).

Measurements of Single Electrons

Electrons are collected by proportional counters so as to produce an electrical pulse whose height is proportional to the number collected. Pulses produced by fewer than about five electrons are subject to nonlinearities due to statistical fluctuations in gas multiplication. Therefore, when fewer than five electrons are collected within a detection cell, the algorithm substitutes an average number between 1 and 4 for these cells.

Spatial Resolution

The choice of using a 10 x 10 array of electrodes in the XY collection plane, as well as a time resolution corresponding to 1 cm electron drift in the Z direction, limits the resolution of single electron coordinates to within one of a thousand 1 cm^3 subvolumes. To reconstruct an ionization track, one can assume that all electrons created in a cell are located at the center of that cell. Reconstructed tracks are then formed from 1000 integers associated with points equally spaced 1 cm apart in all directions.

The dosimeter's algorithm must determine track endpoints in order to calculate track lengths. The algorithm first determines the two cells thought to contain the true endpoints, which are then considered to be located at the cell centers. If a correct cell is chosen, the true endpoint can lie anywhere within that 1 cm^3 cell. Endpoint estimates, therefore, can be off by as much as 0.87 cm, the distance between the cell center and one of its corners. If adjacent

cells are incorrectly chosen, errors in endpoint estimates will be worse. Results show, however, that this resolution is still adequate for neutron dosimetry purposes.

An additional consideration in design is that, once a detector such as this is constructed, the spatial resolution it provides in the XY plane is fixed. If subsequent applications require changes in this resolution, another detector must be built.

Electron Diffusion During Collection

Thermal diffusion of the electrons during their drift through the counting gas can adversely affect the spatial resolution for determining original electron positions within a track. The greater the original Z coordinates of the electrons, the greater will be the amount of diffusion before they are collected. As a result, some electrons will "cross over" into another cell during the time between their creation and their collection. Turner has shown that, for pressure ranges from 1 to 100 torr, diffusion effects are minimized at E/P ratios of 0.4 to 1.0, where E is the field strength in volts/cm and P is the gas pressure in torr (Tu85a). Since the present detector design calls for a gas pressure of 10 torr, the field strength is set at 10 volts/cm to minimize diffusion.

Figures 8 and 9 correspond to those items presented in Figures 4 and 5 for the 500 keV proton, except that the Monte Carlo code displaced the XYZ coordinates of each electron in a Gaussian fashion, simulating the effect of

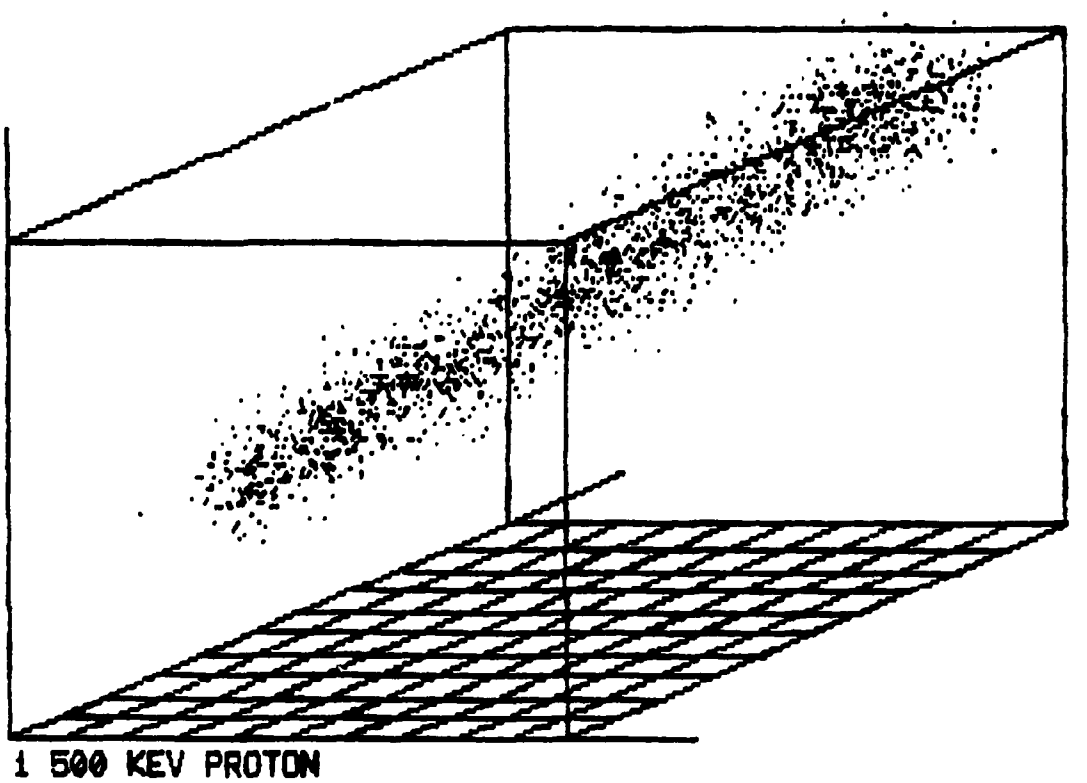

Figure 8. Proton track shown in Figure 4 with electron diffusion simulated.

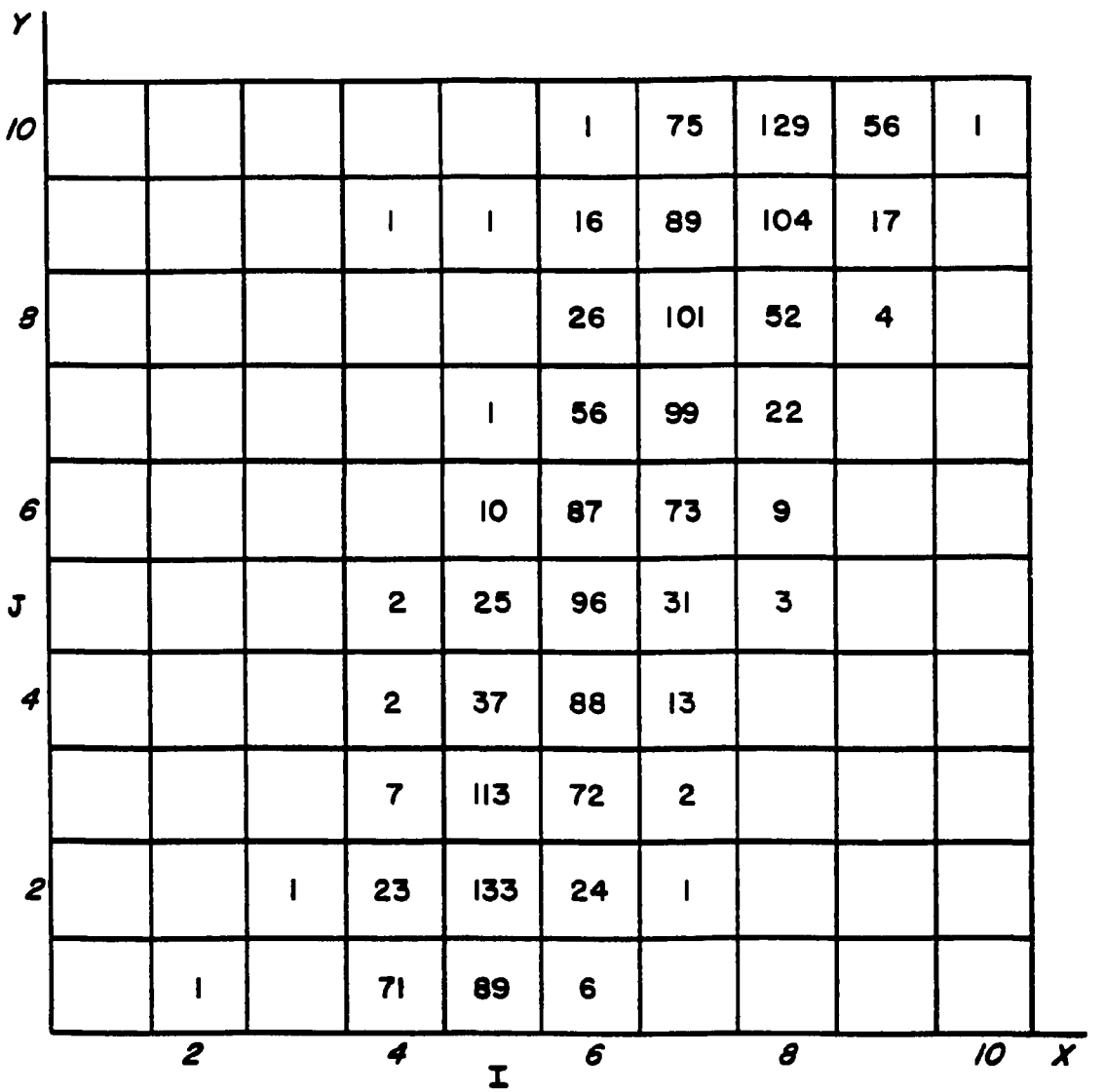

Figure 9. Numbers of electrons produced by the 5ØØ keV proton which are registered within the XY collection plane after thermal diffusion.

diffusion upon track reconstruction. Figures 10 and 11 show how diffusion affects the 80 keV carbon track.

Diffusion decreases detector resolution with respect to reconstruction of the original recoil track. The uncertainties in track-endpoint determination mentioned above are increased, leading to greater uncertainties in measured track lengths. In addition, diffusion effects can also hinder attempts at estimating the energy deposited. Energy deposition is primarily determined from the number of electrons produced within the sensitive volume; therefore, any loss of electrons from that volume due to diffusion will lead to an underestimate of absorbed dose. Two principal configurations for diffusion losses are "axial losses" and "radial losses," where axial and radial refer to the apparent direction of these losses with respect to the track structure after reconstruction.

Axial losses occur when a track enters and exits the sensitive volume in a direction somewhat perpendicular to its boundaries. If these faces coincide with the inside walls of the detector, a large fraction of the electrons found within the core of the track will be lost to the wall surface as they diffuse during their drift to the collection plane. These loses can be substantial for tracks produced by high-energy particles. This effect is minimized by isolating the sensitive volume from the inside walls by a 2-cm buffer region between the detector wall and the boundary of the sensitive volume. Needle electrodes would be placed uniformly within this buffer region in order to collect

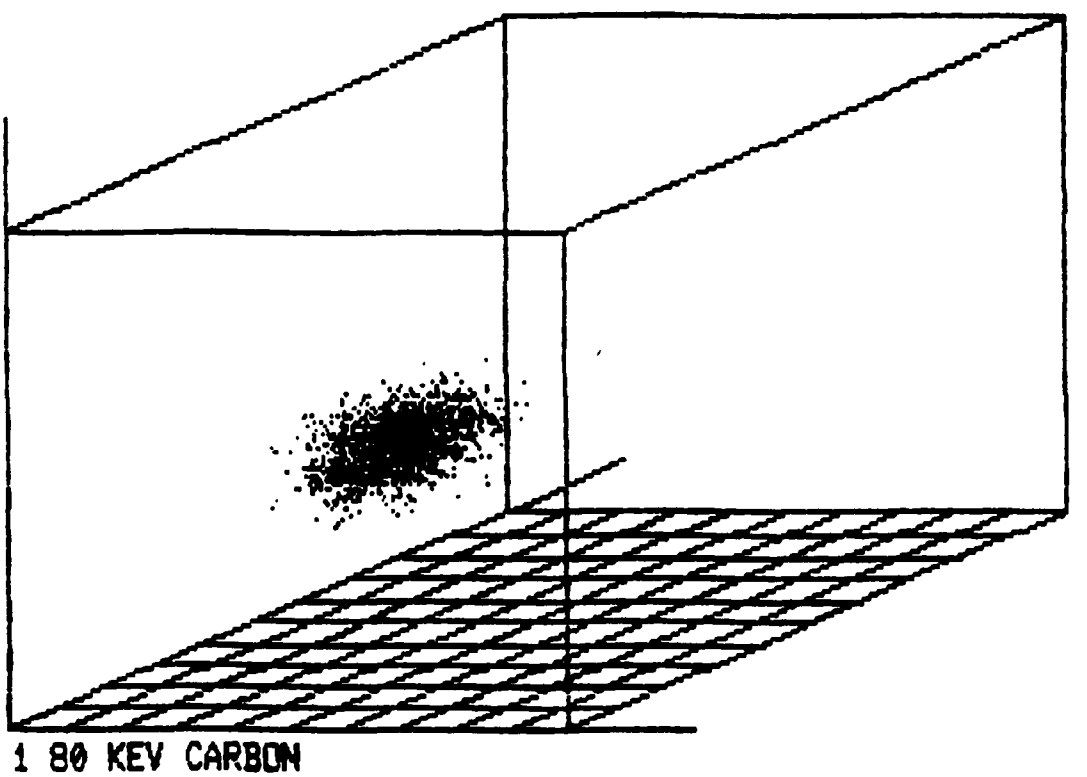

Figure 1Ø. Carbon ion track shown in Figure 6 with electron diffusion simulated.

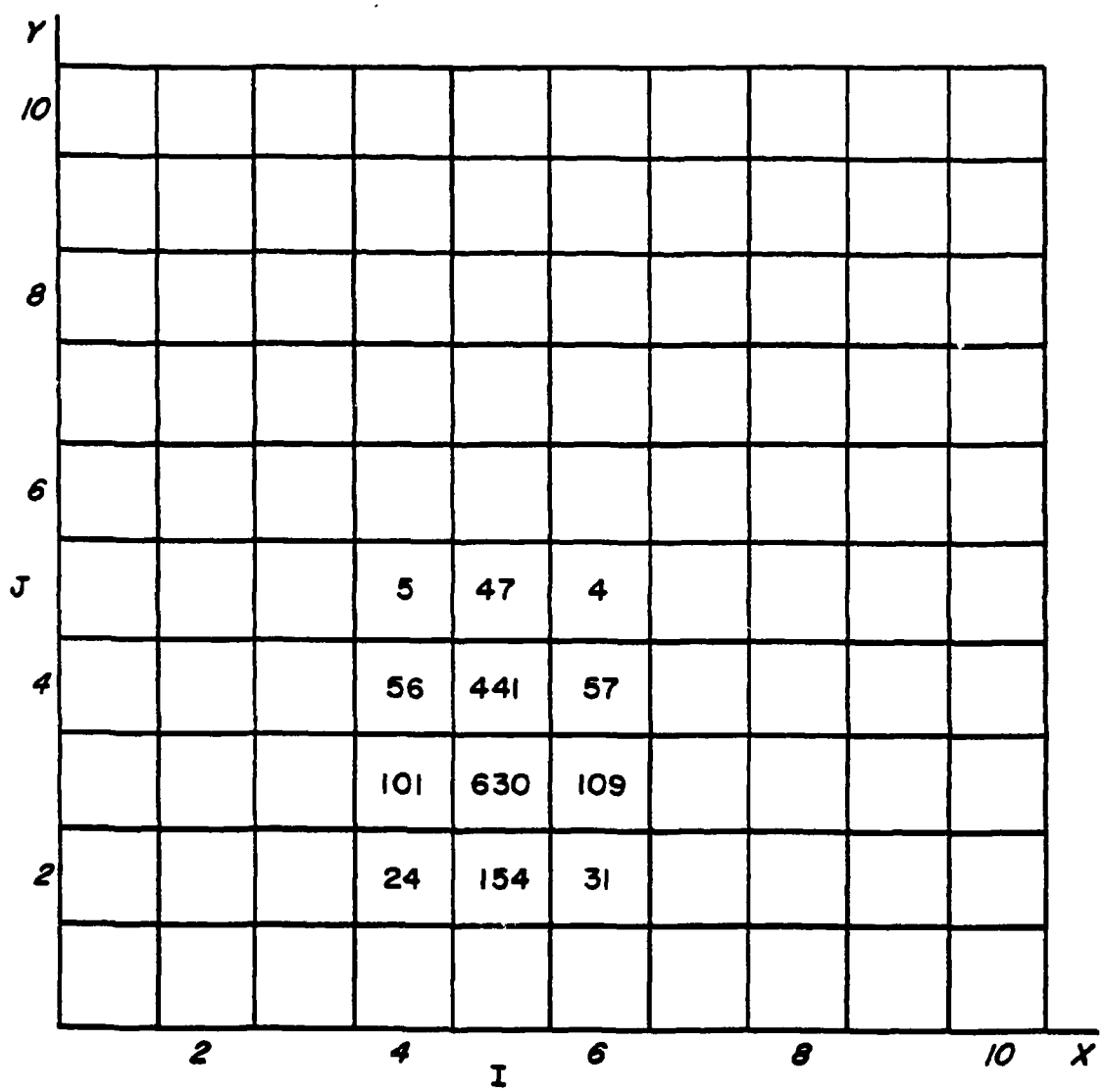

Figure 11. Numbers of electrons produced by the 80 keV carbon ion which are registered within the XY collection plane after thermal diffusion.

electrons created within this portion of the gas volume. Their resulting pulses, however, would not contribute to the 1000 integer response the detector. Within this buffer region, every electron created within the sensitive volume which would diffuse to the buffer during its drift, a similar electron would diffuse into the sensitive volume from the buffer region. Compensation would be established for what would have been wall losses.

The revised chamber design is given in Figure 12. The sensitive volume now lies between 2 and 12 cm in the X and Y directions, yet the cell indices i and j still run from 1 to 10 with respect to the sensitive volume. No buffer region was added in the Z direction since displacement in this direction is a displacement in arrival time, resulting in no reduction of the number of electrons collected. By adding the buffer region, one is compromising detection of low-energy recoils from the inner wall surfaces which cannot reach the sensitive volume for correct analysis of tracks which are able to cross the chamber. This situation will possibly lead to dose estimates at low energies principally from analysis of inners.

Radial diffusion losses occur for the complimentary track orientation where the particle traverses the sensitive volume in a direction somewhat parallel to one of its boundaries. A certain fraction of the electrons along the outer regions of the track core will be lost to the either the detector wall if no buffer is in place, or to the buffer if one exists. For these radial losses, the buffer region

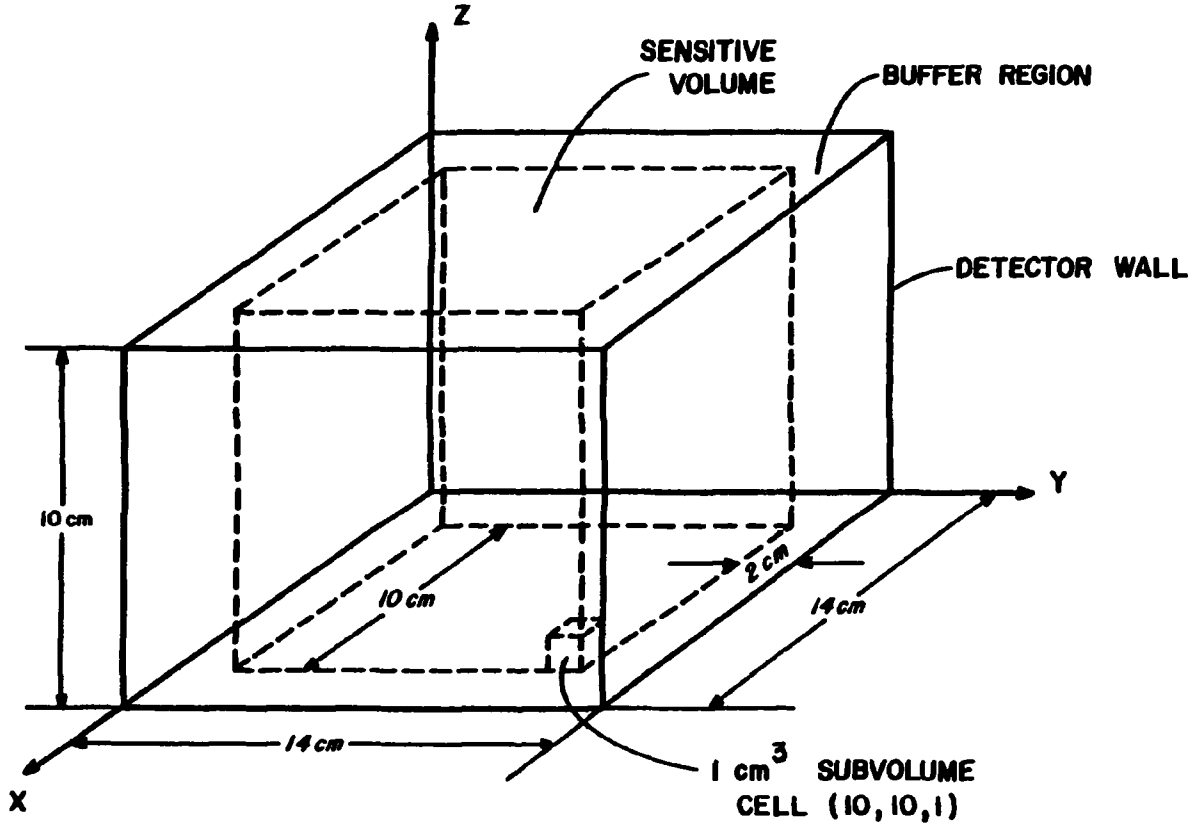

Figure 12. Final detector design.

provides no compensation. For tracks exhibiting potentially large radial diffusion losses, it is up to the algorithm to decide whether or not the track should be analyzed. Such questionable tracks are referred to by the algorithm as "skimmers." Recoil particles running parallel to and outside of one face of the sensitive volume can send electrons into that volume via diffusion. This collection of electrons inside the sensitive volume will appear to the algorithm as a track produced by a lower LET particle. Therefore, the choice of analyzing skimmers involves both risks of dose underestimation by not analyzing skimmers truly produced within the sensitive volume, versus dose overestimation by analyzing these apparent tracks produced from electrons created by recoil particles outside the sensitive volume. For a uniform distribution of recoil tracks within the gas volume, compensating errors may be realized.

Relative Z Coordinates

Although not explicitly stated, it is assumed that the proposed proportional counter has no mechanism to time the actual occurrence of each event within the sensitive volume. Any data acquisition will thus begin only after the arrival of the first electron at its respective electrode. This time delay profoundly affects the determination of electron Z coordinates since they are inferred by arrival times. Z coordinates are therefore not relative to the XY collection plane, but are relative to the absolute Z coordinate of the

lowest electron created in the track. Two events identical in track length and direction, but differing in their height above the collection plane will therefore be indistinguishable to the detector and thus to the algorithm.

For a majority of cases, the algorithm's use of relative rather that absolute Z coordinates will have no effect on its results. However, as explained in Chapter 3, the algorithm's treatment of inners differs from its treatment of stoppers and starters for both protons and especially carbon tracks. For events yielding no triggered cells at i and j equaling 1 or 10, the algorithm must decide to analyze these tracks as inners or as stopper/starters, since true inners are indistinguishable from tracks entering or exiting the upper or lower faces of the sensitive volume. It is reasonable to assume that the choice should depend upon the energy of neutrons encountered, where at low energies inners are predominant, and at high energies stoppers and starters are predominant.

Energy Loss and Range Straggling

Limitations beyond the control of any detector result from inherent fluctuations in both range and energy deposition by identical charged particles. Energy loss by charged particles is a stochastic process due to the random nature of the microscopic interactions they undergo during their traversal of a medium. The amount of energy lost by a particle for each excitation or ionization event encountered varies in a probabilistic fashion. As a consequence, there

exists a distribution of ranges for equally energetic inners and stoppers and a similar distribution of energy depositions for equal starter and crosser track lengths. Due to the course spatial resolution of the proposed detector, range straggling on the order of a few tenths of a centimeter should not be a problem. For detector designs with improved spatial resolution for use in microdosimetry, range straggling would be a concern. Diffusion losses overshadow energy-loss straggling in the current detector design.

CHAPTER 3

DESCRIPTION OF NEUTRON DOSE ALGORITHM

The next step in the dosimeter design was the development of an algorithm which, when given digital track-structure information as described in Chapter 2, would unfold absorbed dose, LET, and dose equivalent. The algorithm development proceeded with the aide of ORNL's Monte Carlo code which transports both proton and carbon recoils through methane. The code tabulates the energy deposited and the number of subexcitation electrons produced in each of the 1000 cells within the sensitive volume. The code then diffuses these electrons in a Gaussian fashion to simulate their displacement during collection drift. Additionally, datafiles are created giving the XYZ electron coordinates both before and after diffusion. It is with this latter datafile that the FORTRAN version of the algorithm, presented in this chapter, begins its data analysis.

Algorithm Program Structure

The algorithm portion of ORNL's neutron dosimeter was developed as a FORTRAN program consisting of a main program segment (NDOSE) and nine subroutines (FILSUM, SKIMER, SEARCH, LENGTH, PCRNGE, CARBON, WHICH1, DEQUIV, and ABORT). The logic of the algorithm's subroutine calls is given in the form of a flow chart shown in Figure 13. The data analysis is performed in two segments, hereafter designated

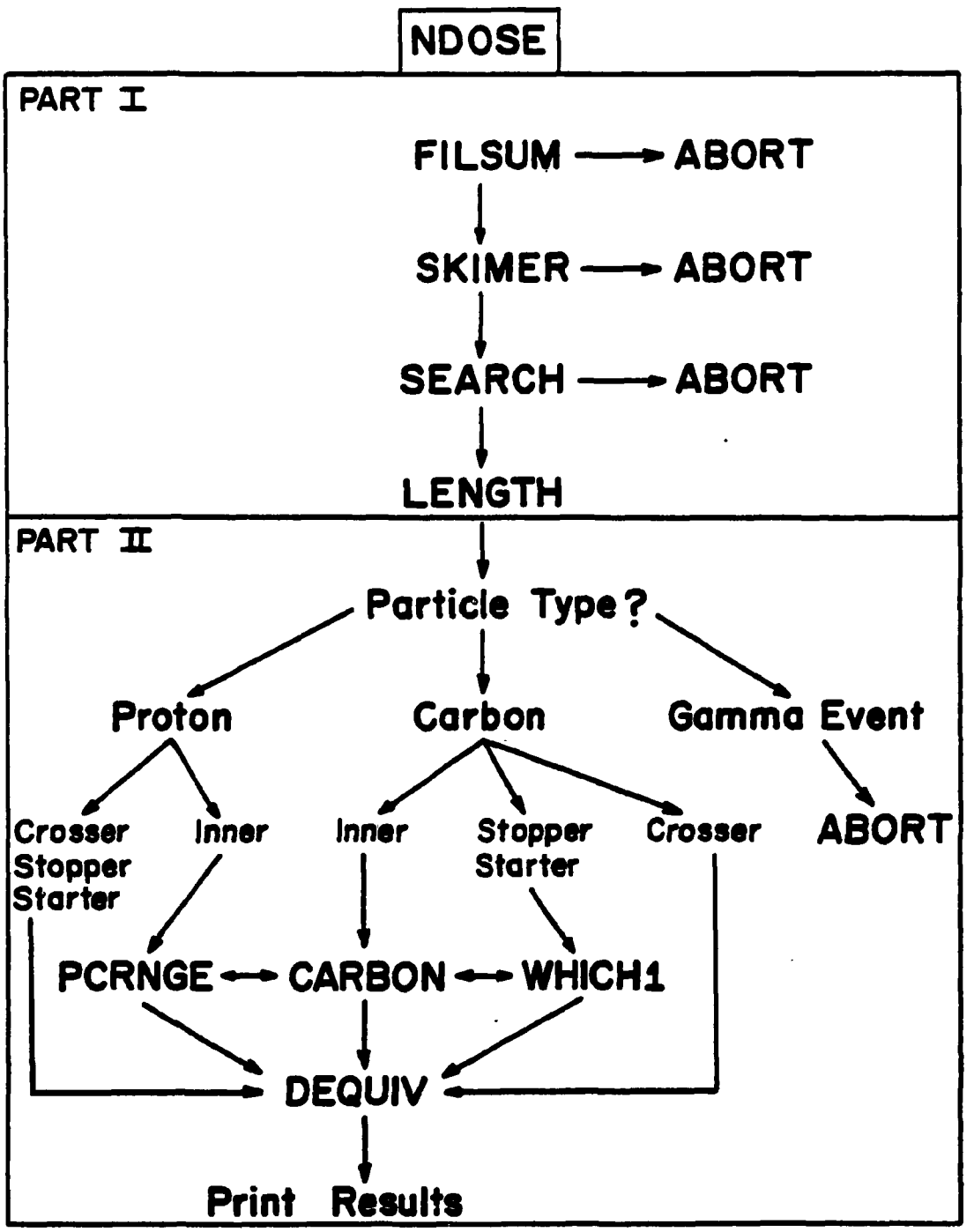

Figure 13. Algorithm flow chart.

as Part I and Part II. Part I is performed uniformly for all tracks detected and consists of consecutive calls to subroutines FILSUM, SKIMER, SEARCH, and LENGTH. FILSUM provides the link between the exact XYZ electron coordinates after diffusion provided by the Monte Carlo simulation code, and the proposed 1000 integer response of the proportional counters. Additionally, FILSUM determines the total number of electrons produced in the sensitive volume. SKIMER tests to see if the analysis should be aborted due to the effects of "radial" diffusion losses discussed in Chapter 2. Subroutines SEARCH and LENGTH together determine the length of the recoil track segment within the sensitive volume.

With a detector exhibiting a fine spatial resolution, determination of track endpoints would be straightforward. Given the coarse spatial resolution of the proportional counter, however, precise determination of track endpoints can only be accomplished through elaborate methods of track reconstruction. This would involve converting the 1000 integer array given by the detector into the actual XYZ coordinates of each electron. Such a process could be aided by performing a three-dimensional linear regression of the centers of all triggered cells weighted by the number of electrons they contain. In addition, diffusion effects will distort the pattern of triggered cells, further complicating reconstruction attempts.

Such a reconstruction effort would represent overkill for the purposes of neutron dosimetry. Instead, the algorithm uses subroutine SEARCH to determine which two cells

most likely contain the true endpoints, and subroutine LENGTH calculates track length given the spatial location of those cells.

Part II of the analysis begins by determining if the track was created by a recoil proton, a carbon ion, or an electron, the latter produced by a gamma events. Once the particle type is known, NDOSE, with the aide of subroutines PCRNGE, CARBON, and WHICH1, determine energy deposition and LET. Subroutine DEQUIV then calculates the track's contribution to the total dose equivalent. NDOSE then prints the final output consisting of electron number, energy deposition, track length, LET, and dose equivalent from both the Monte Carlo code (actual) and the algorithm (inferred), giving the corresponding percent difference for each quantity.

Data Analysis - Part I

Subroutine FILSUM

The output of the proposed neutron detector based upon proportional counting would consist of 1000 integers, each giving the inferred number of electrons, after diffusion, contained within the 1000 cells of the sensitive volume. Since the Monte Carlo code gives the exact XYZ coordinates of these electrons (mainly for plotting purposes), FILSUM's first task is to recreate those 1000 integers. Initially, the datafile is read to determine the electron with the lowest Z coordinate after diffusion. Assuming no prompt triggering mechanism exists to inform the detector that an

event has occurred, the datafile is reread to generate relative Z coordinates by subtracting this minimum Z value from each Z coordinate read.

It is possible that, after accounting for diffusion, the Monte Carlo code would relocate electrons to points below the XY collection plane such that their Z coordinates would be less than zero. Physically, this situation describes electrons drifting to the collection plane at a velocity above the average drift velocity. If such Z values are found, they are set equal to zero.

FILSUM continues by tabulating the numbers of electrons within each of the 1000 cells. Electrons with negative Z coordinates are assumed to be collected along with all other electrons located within the first centimeter above the collection plane. Electrons with relative Z coordinates greater than 10 cm, as generated by tracks such as vertical crossers, are assumed not collected within the sensitive volume.

Once the number of electrons within all 1000 cells are tabulated, the array is then searched for cells containing electrons numbering less than the variable LOWNUM, which is currently set at 5. As discussed in Chapter 2, pulses produced by such low numbers of electrons are subject to nonlinearities; therefore, the numbers of electrons contained in these cells are set equal to the variable AVGNUM. AVGNUM represents the average value of all cells containing less than LOWNUM electrons, where this average is currently set at 2. Such a substitution procedure could be

accomplished by the detector through use of a lower level discriminator setting.

Up to this point, FILSUM has essentially functioned to simulate the electronic output of the proportional counter by generating a 1000 integer array. Previously, the Monte Carlo program had simulated the track creation and also the diffusion of electron coordinates due to collection by proportional counting. Probably a more logical arrangement would have coordinate diffusion performed not within the Monte Carlo code, but within subroutine FILSUM. The resulting organization would have the Monte Carlo code simulate only the physics of recoil track creation. Once a collection method is decided upon, its simulation would be accomplished entirely within subroutine FILSUM.

Finally, subroutine FILSUM sums the contents of all 1000 cells to estimate the total number of electrons created within the sensitive volume. This number will in general be lower than the actual number created depending upon the magnitude of diffusion losses.

Subroutine SKIMER

Before proceeding further, the algorithm at this point must decide whether "radial" diffusion losses could be substantial enough to warrant aborting the analysis. Radial losses are important for tracks running somewhat parallel to one of the faces of the sensitive volume, where these track orientations are termed "skimmers." Skimmers can account for underestimating absorbed dose from proton or carbon

tracks, misidentification of carbon tracks as proton tracks, and inclusion of apparent tracks from electrons created by recoils outside the sensitive volume.

Tracks are labeled as skimmers by subroutine SKIMER through determining the percentage of electrons contained within cells bordering the buffer region and also the number of bordering cells triggered. SKIMER begins by summing the number of electrons contained within all cells within the I=1, I=10, J=1, and J=10 slabs. The K=1 and K=10 slabs are not included in this sum with the argument that vertical diffusion effects cause displacements in electron collection-times and thus do not constitute a physical loss mechanism. This sum is then divided by the total number of electrons within the sensitive volume to obtain the fraction of electrons found within cells bordering the buffer region. If this fraction is above the cutoff value given by variable SKIMCO, the track is up for consideration as a skimmer. If the fraction is below SKIMCO, the track "passes" the skimmer test and subroutine SKIMER is exited.

The value of SKIMCO was determined so that all proton tracks exhibiting a percentage of electrons within border cells greater than SKIMCO would produce a greater than 10% underestimate in energy deposition. To determine this cutoff value, five proton tracks were run parallel to the Y-axis and, to increase diffusion effects, at a height of 8.5 cm. The starting X coordinates were 10.8, 11.0, 11.2, 11.4, and 11.6 cm respectively, drawing the track closer and closer to the X=12.0 cm face of the sensitive volume. The

results are shown in Table 3. A 10% error in energy deposition occurred approximately at a percentage of 65%, and SKIMCO was thus set at 65%.

TABLE 3
Determination of SKIMCO

Starting X (cm)	% Error in Energy Deposition	Percentage of Electrons within Border Cells
10.8	3.7	47.5
11.0	8.2	59.0
11.2	10.5	67.3
11.4	18.2	74.8
11.6	26.6	83.3

The second criterion which a track must meet to be labeled a skimmer is that the number of triggered cells within either the I=1, I=10, J=1, or the J=10 slab must exceed the variable NBOXCO. This additional test was added so that short tracks which enter the sensitive volume somewhat perpendicularly to one of its faces will not be discarded. Since these tracks trigger approximately nine cells which border the buffer region (there are at most eight cells adjacent to a given cell within a slab), NBOXCO was set at 9 cells. If this second criterion is meet, subroutine SKIMER calls subroutine ABORT which performs cleanup operations and aborts the analysis. If not, this track also "passes" the skimmer test and control is returned to the main program NDOSE.

By selectively discarding certain questionable tracks in this manner, one is accepting a loss of efficiency in order to be correct on a track-by-track basis. One could also make the argument that by excluding the skimmer test, dose underestimates would be somewhat compensated for by dose overestimates. Dose underestimates would arise from analyzing tracks subject to "radial" diffusion losses. If these losses are substantial, the algorithm at some point will analyze high LET carbon tracks as lower LET proton tracks, also contributing to dose equivalent underestimates. Dose overestimates would occur from analysis of apparent tracks generated by high-energy recoils outside the sensitive volume.

Subroutine SEARCH

This subroutine determines which two cells of the 1000 cell array are most likely to enclose the true endpoints of the track. The routine begins by considering the 10 by 10 array of integers within the J=1 slab of the sensitive volume. This 100 integer array is searched to determine the cell containing the greatest number of electrons provided that number exceeds the variable LOWNUM. The requirement that an endpoint cell must have greater than LOWNUM electrons insures that false endpoints caused by track extension from diffusion effects will be avoided. If no cells contain at least LOWNUM electrons, the search is advanced inward to the J=2 slab where this 100 integer array is scanned for a maximum cell content. This scanning of slabs parallel to

the XZ face continues until a endpoint cell candidate is found. If the search continues all the way to the J=1Ø slab without locating a single candidate cell, subroutine ABORT is called, ending the analysis. If a candidate cell is located, SEARCH repeats the search in the reverse direction starting with the J=1Ø slab. Since the first search follows along the positive Y direction and the second along the negative Y direction, these two scans are respectively referred to as the positive and negative XY searches.

The four remaining candidate cells are found in a similar fashion from a positive YZ search starting with the I=1 slab, a negative YZ search starting with the I=1Ø slab, a positive XY search starting with the K=1 slab, and a negative XY search starting with the K=1Ø slab. The next decision to be made is which 2 of the 6 cells contain the true track endpoints. The choice is simple if one has prior knowledge of track orientation. As an example, consider a crosser which enters the sensitive volume at the center of its Y=2.Ø cm face and runs parallel to the Y-axis. The two optimal choices would be the cells chosen from the positive and negative XZ searches. The YZ and XY searches would more than likely locate cells interior to the cube radially located from the core of the track. Similar arguments can be made for tracks running parallel to the X and Z axes.

Other track orientations can further complicate the decision. Consider a crosser also starting at the center of the Y=2.Ø cm face of the sensitive volume but exiting through the center of the X=12.Ø cm face. The optimal

choices for endpoint cells in this case would be the cells chosen from the positive XZ search and the negative YZ search. Since the algorithm would hopefully operate independent of recoil direction, a consistent method of choosing the best 2 of 6 candidate cells must be implemented.

Experience has shown that errors in track-length estimations are minimized if the algorithm chooses the cell pair whose centers form the longest chord within the sensitive volume. Given this information, SEARCH calculates chord lengths between the centers of all 15 cell pair combinations; the pair forming the greatest cord length is designated as the two chosen endpoint cells. If all chord lengths are zero, then the track is contained entirely within a single cell, and the analysis is aborted.

SEARCH, before returning control to NDOSE, classifies the track as a crosser (C), an inner (I), or a stopper/starter (S), based upon the (I,J) indices of the endpoint cells just determined. For instance, if a track had one endpoint cell with an I or J index equaling 1 or 10, while the second endpoint cell had an I or J index not equaling 1 or 10, this track configuration would be either a stopper or a starter.

The K indices of the endpoint cells are not considered since the use of relative Z coordinates prohibits the distinction between inners and starter/stoppers exiting or entering the upper or lower XY faces of the cube. Such orientations are assumed by default to be inners. Only when

the two K indices of the endpoint cells are 1 and 10 is one assured that the track completely traversed the sensitive volume in the vertical direction; in these cases, the track is logically labeled a crosser.

Subroutine LENGTH

Ending Part I of the algorithm, subroutine LENGTH takes the (I,J,K) locations of the endpoint cells found in SEARCH and estimates track length as the chord length between their centers. If a track is a stopper/starter or a crosser such that at least one endpoint cell lies within either the I=1, I=10, J=1, or J=10 slabs, the track length chord is extended to the intersection of the corresponding XZ or YZ face of the sensitive volume. The final track-length estimate is then returned to NDOSE.

Data Analysis - Part II

Determination of Particle Type

Having determined the number of electrons created and the track length of the recoil event within the sensitive volume, one can distinguish carbon ion from recoil proton events given physical data expressing how these recoils expend energy in methane. Such physical data have been compiled and are given in Figures 14 and 15. Figure 14 gives average W-values as a function of recoil energy for both protons and carbons ions in methane (ICRU79). The proton W-value is essentially constant at 30 eV/ip, while the carbon W-value increases with decreasing carbon energy. Figure 15 gives mass stopping power as a function of recoil

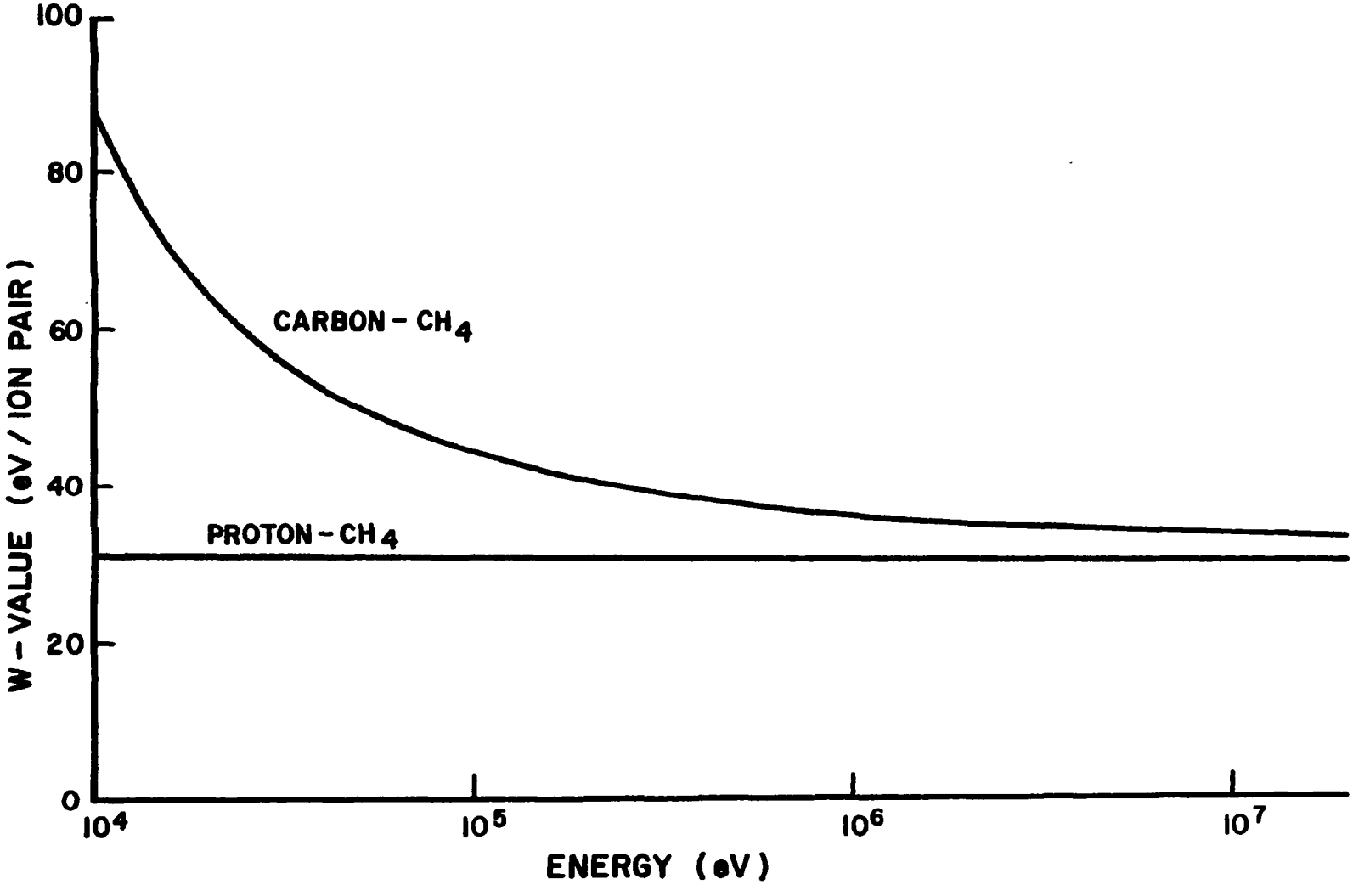

Figure 14. Proton and carbon ion W-value in methane.

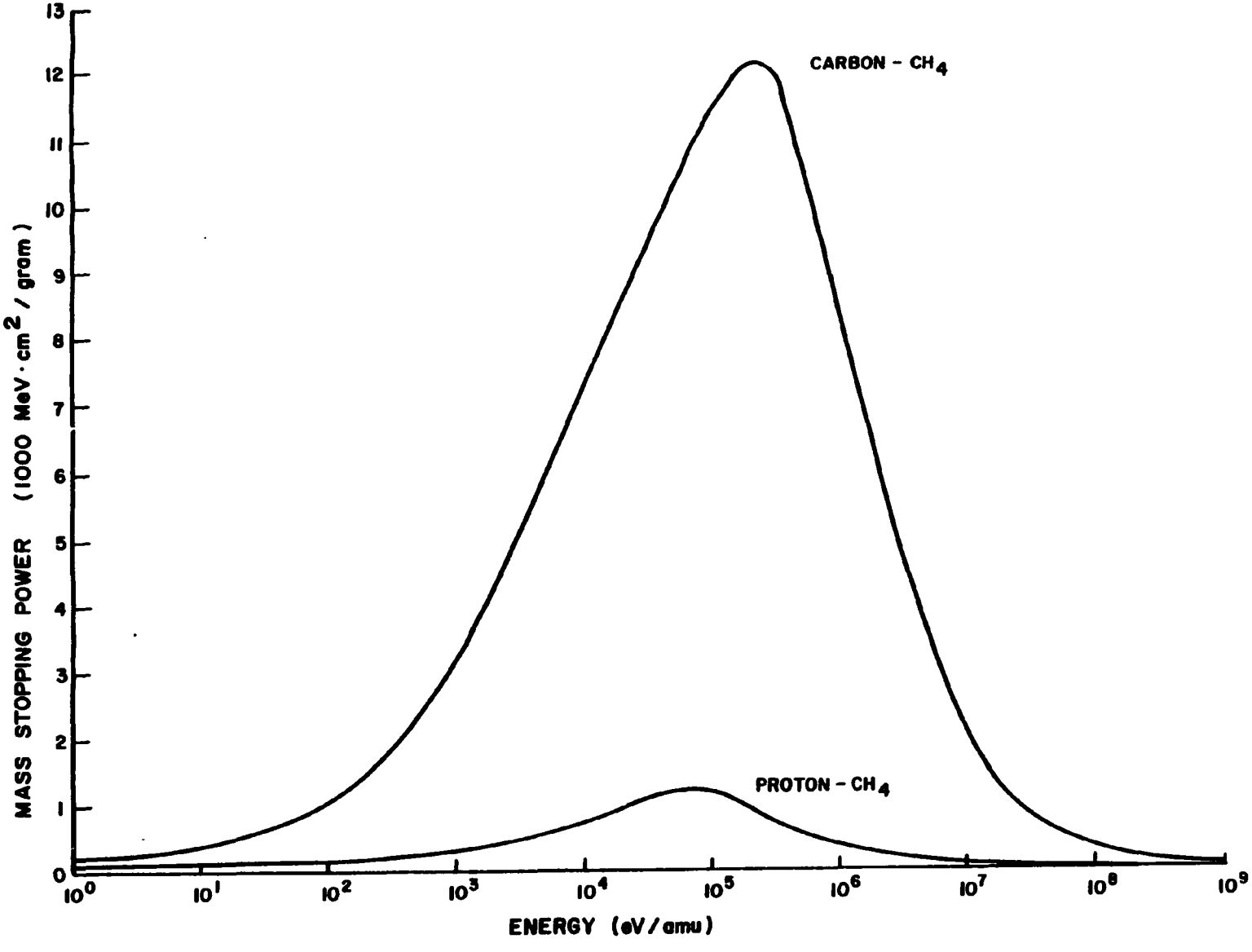

Figure 15. Mass stopping power for protons and carbon ions in methane.

energy for both protons and carbons in methane (NAS64). In contrast to the carbon curve, proton mass stopping power remains fairly energy independent, reaching a peak value (Bragg peak) of only 1.2 x 10^3 MeV·cm^2/g. The peak of the carbon curve reaches 12.2 x 10^3 in those same units. Except at low energies, the average mass stopping power attained by carbon ion track-segments within the sensitive volume will exceed 1.2 x 10^3 MeV·cm^2/g, and thus the difference between the proton and carbon Bragg peaks in methane provides a natural discriminator between these two recoil events.

Utilizing the above information, NDOSE proceeds to calculate an average mass stopping power for the track assuming that it was created by a proton. Specifically, the number of electrons collected is divided by the track-length estimate to obtain an average specific ionization in eV/cm. Next, this value is multiplied by the constant 30 eV/ip for protons, eV converted to MeV, and the result divided by 1000 to obtain an average mass stopping power in 1000 MeV·cm^2/g. If this value exceeds 1.2, the track is labeled a recoil carbon; if between 1.2 and 0.02 the track is designated a recoil proton.

Discrimination of single gamma events is accomplished by aborting the analysis if the average mass stopping power calculated above is less than 20 MeV·cm^2/g. However, pulse pileup from several gamma events can only be acknowledged by a more sophisticated algorithm capable of spatially separating such events.

Proton Analysis

Techniques of estimating energy deposition and thus linear energy transfer differ depending upon particle type as determined by NDOSE. This subsection will describe analyses of proton tracks, while the following subsection will discuss treatment of carbon tracks.

Energy deposition by all proton tracks is determined by NDOSE as the product of the number of electrons created within the sensitive volume and the constant proton W-value in methane, 30 eV/ip. If SEARCH had determined the track was a crosser or a starter/stopper, a track average LET in units of MeV·cm^2/g is determined by dividing energy deposition in MeV by track length in cm and then by the gas density in cm^3/g. The energy deposition and LET are then passed to subroutine DEQUIV, discussed later in this chapter, which passes back to NDOSE the event's contribution to the total dose equivalent. The final results given by NDOSE include number of electrons created, energy deposition, track length, LET, and dose equivalent contribution for the track as determined by the Monte Carlo code and as inferred by the algorithm, as well as percent differences for each quantity.

For reasons relating to the poor spatial resolution of the current chamber design, the track-length estimate for proton inners as determined by subroutine LENGTH is replaced by a more accurate estimate obtained by NDOSE from a call to subroutine PCRNGE. With inners, tracks are completely confined within the sensitive volume and one is assured that

the recoil's total initial energy was deposited within that volume. A curve giving range versus initial recoil energy is thus used to obtain a more accurate track-length estimates. PCRNGE accesses datapoints tabulated from the proton range curve shown in Figure 16. This curve was generated by integrating the inverse of the proton mass stopping power curve from zero to different values of initial recoil energy and normalizing to a pressure of 10 torr. PCRNGE determines proton range by a logarithmic linear interpolation between pairs of initial energy and corresponding range in methane. Track average LET is then calculated using this new value of track length, and the dose equivalent contribution is given by subroutine DEQUIV as was done for the other track orientations.

Carbon Analysis

If a track is designated a carbon inner, NDOSE calls subroutine CARBON to obtain estimates of energy deposition and track length. As with the proton inners, one is assured that the recoil's total energy was deposited within the sensitive volume. Since the W-value for carbon recoils is a function of initial recoil energy, CARBON uses a plot of cumulative ion pairs produced by carbon ions in methane versus initial energy, shown in Figure 17, to obtain energy deposition. Figure 17 was generated from quotients of initial energy by W-value given in Figure 14 with values below 10 keV obtained by extrapolation. Subroutine CARBON thus obtains energy deposition by linear interpolation

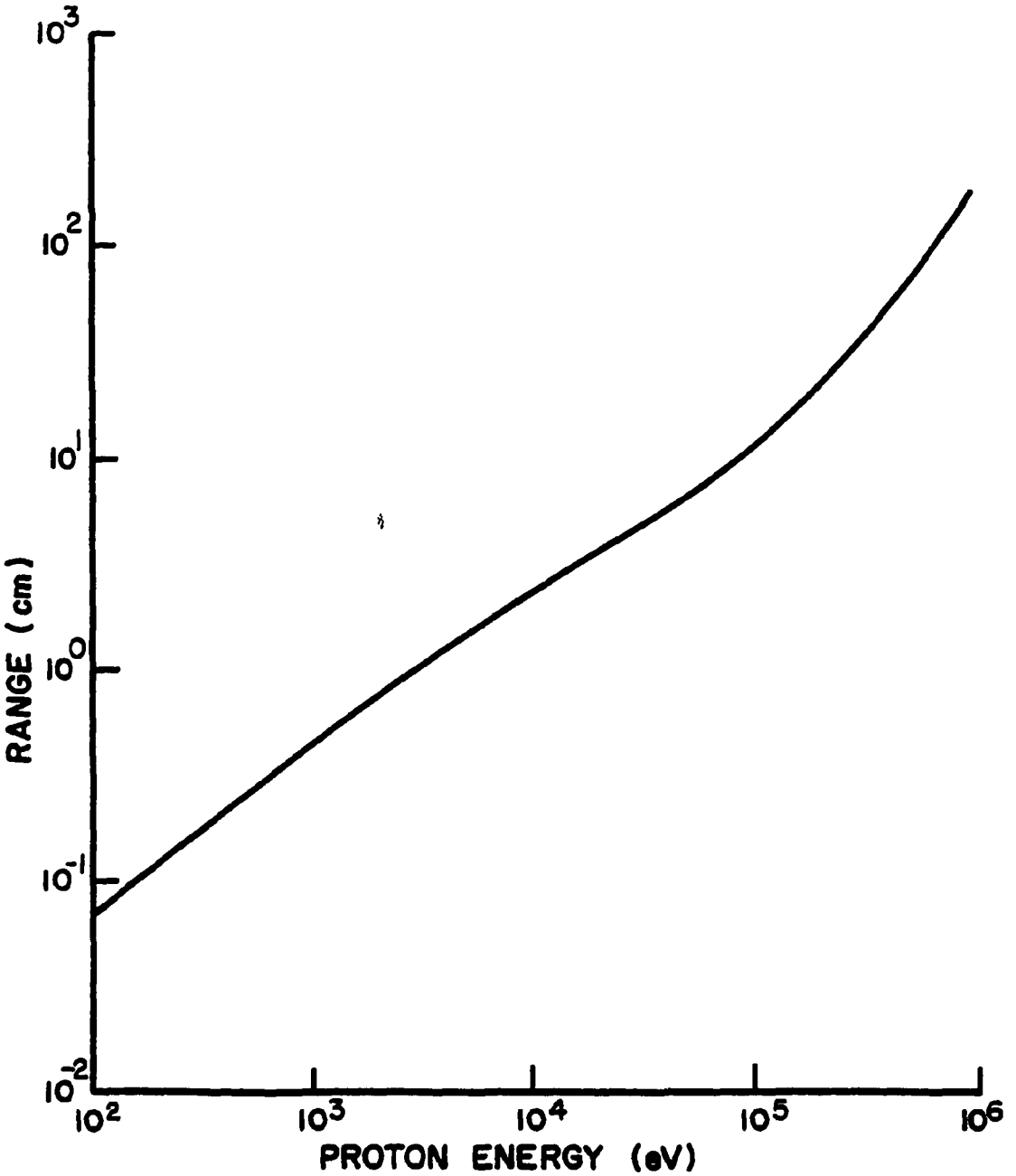

Figure 16. Proton range in methane at 1Ø torr.

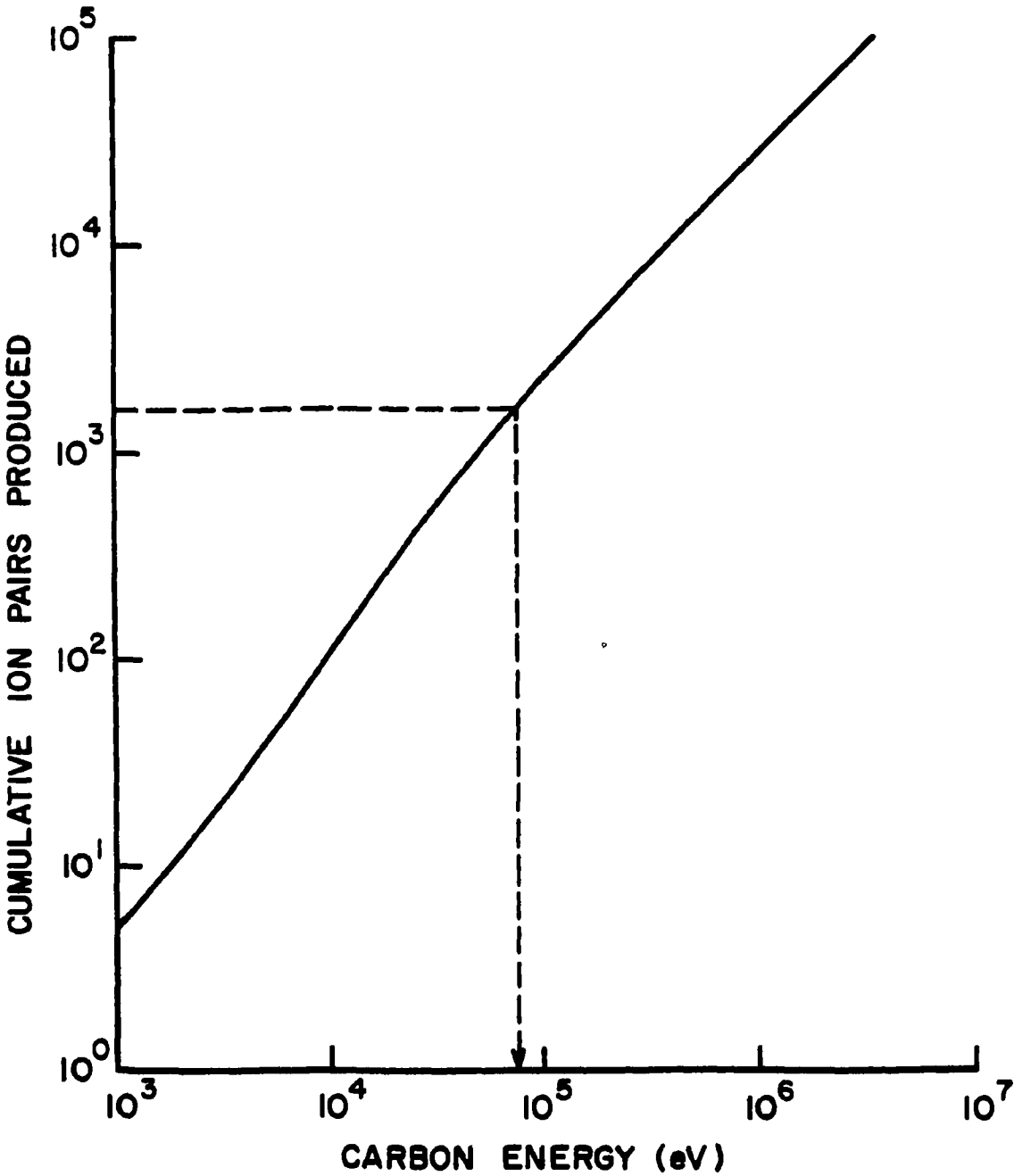

Figure 17. Ion pair production by carbon ions in methane.

between data pairs tabulated from Figure 17. Subroutine CARBON then calls subroutine PCRNGE which accesses a range curve for carbons in methane at 10 torr, shown in Figure 18, to obtain an updated estimate for track length. Figure 18 was generated in a manner similar to that used to create Figure 16. Both energy deposition and track length are then returned to NDOSE, LET is calculated, and DEQUIV determines dose equivalent contribution from the carbon inner.

If a track is designated a carbon crosser, energy deposition is determined by the product of the number of electrons collected and an average W-value for high energy carbons. Use of such an average is easily justified since Figure 14 shows that the carbon W-value approaches a constant value for increasing carbon energies. To determine an average W-value for all carbon crossers, one must designate the energy range over which the chamber will encounter such events. The lowest energy carbon ion which will completely traverse the 10 cm sensitive volume has an initial energy of 700 keV, given a methane pressure of 10 torr. The highest energy carbon ion produced by a 20 MeV maximum neutron energy has a initial energy of 5.68 MeV. Therefore, an average W-value for all possible carbon crossers is obtained by integrating Figure 14 over carbon energies 700 keV to 5.68 MeV.

Using the following averaging technique,

$$\frac{\int_{E_o}^{E_f} W \, d(\ln E)}{\int_{E_o}^{E_f} d(\ln E)}, \qquad (13)$$

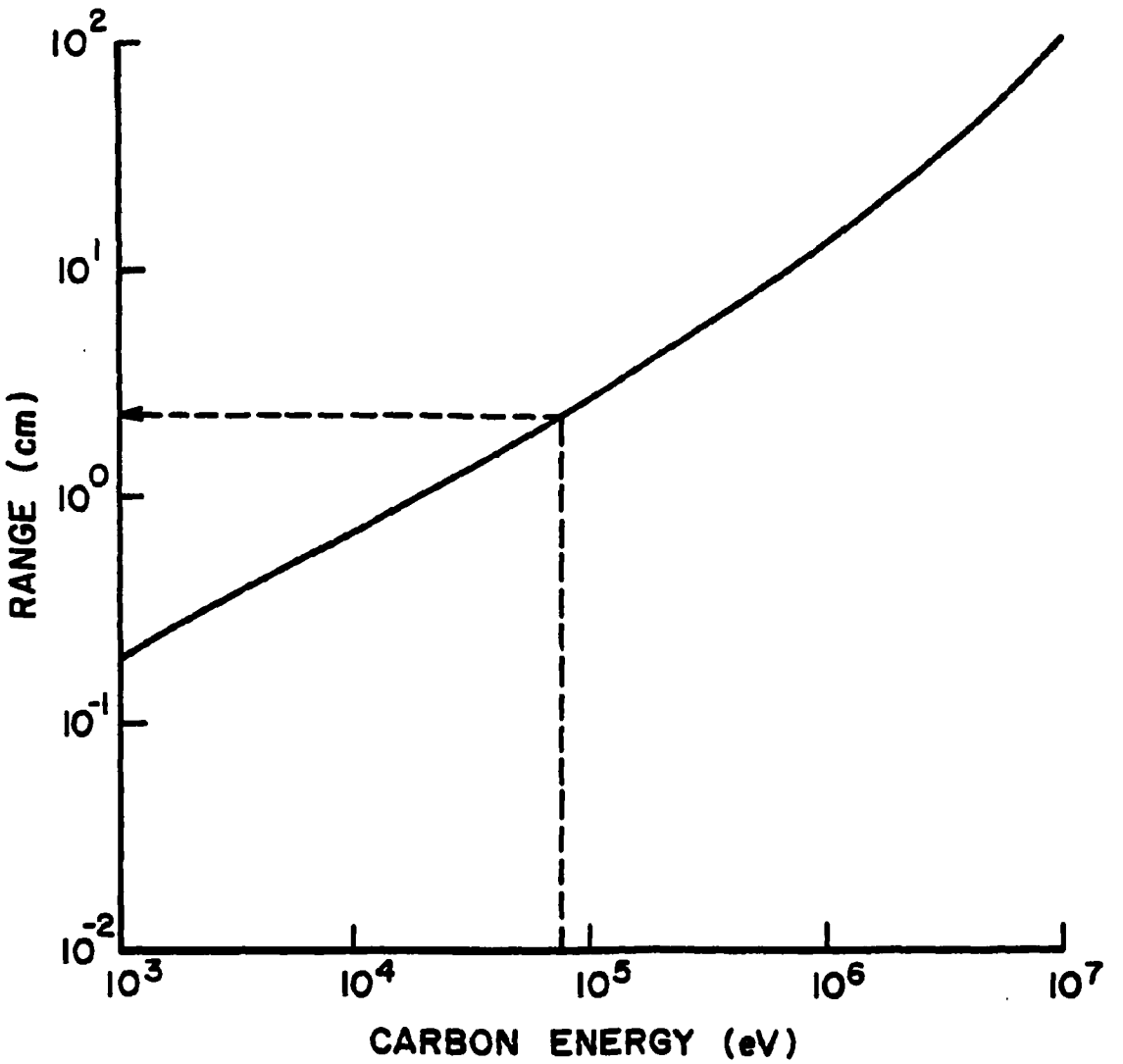

Figure 18. Carbon ion range in methane at 1Ø torr.

where E_o is a variable lower energy bound and E_f is a fixed upper energy bound of 5.68 MeV, Table 4 is produced showing average W-values for various carbon energy intervals.

TABLE 4
Average Carbon W-value from E_o to 5.6 MeV

E_o (eV)	Average W-value (eV/ip)
1.0E+04	46.35
2.0E+04	42.22
3.0E+04	40.88
4.0E+04	40.15
5.0E+04	39.63
6.0E+04	39.24
7.0E+04	38.93
8.0E+04	38.67
9.0E+04	38.46
1.0E+05	38.28
2.0E+05	37.03
3.0E+05	36.34
4.0E+05	35.94
5.0E+05	35.62
6.0E+05	35.37
7.0E+05	35.15
8.0E+05	34.96
9.0E+05	34.79
1.0E+06	34.63
1.5E+06	34.17
2.0E+06	34.01
3.0E+06	33.84
4.0E+06	33.70
5.0E+06	33.71

Table 4 shows that the average W-value for the energy interval 700 keV to 5.68 MeV is 35.15 eV/ip. Energy deposition by all carbon crossers is therefore determined by multiplying the number of electrons collected by 35.15 eV/ip. LET is then calculated by NDOSE using the track-

length estimate given by LENGTH, and the track's contribution to dose equivalent is determined by subroutine DEQUIV.

The third class of tracks the algorithm must consider for carbons is that of stoppers and starters. Unlike the analysis of proton tracks, an attempt is made to distinguish carbon stoppers from carbon starters. One is motivated to make such a distinction since the carbon W-value is energy dependent resulting in different energy depositions for stopper and starter pairs of equal track length. The separation and analysis of carbon stopper and starter tracks is performed by subroutine WHICH1, where this separation is based upon the observation that a high-energy carbon starter, due to its lower W-value, will produce a greater number of ion pairs than a lower energy carbon stopper of equal track length.

Subroutine WHICH1 begins by analyzing the track as if it were a carbon stopper. Assuming all energy transfers occur within sensitive volume and radial diffusion losses are minimal (both generally poor assumptions), energy deposition by stoppers can be determined in the same manner applied to inners. With these assumptions, subroutine WHICH1 sends the number of electrons collected to subroutine CARBON which returns an energy deposition and track length as determined by Figures 17 and 18, respectively. If the original track-length estimate by subroutine LENGTH is equal to CARBON's track-length estimate within a +/- interval of 0.8 cm, the track is labeled a stopper and the values for energy deposition and track length given by CARBON are

passed back to NDOSE so that LET and dose equivalent contribution can be calculated.

If the original track-length estimate falls below this interval, the track is labeled a starter. Energy deposition for carbon starters is calculated as the product of the number of electrons collected and an average W-value for all carbon starters encountered. At the current spatial resolution, the lowest energy carbon starter which can be detected is a 40 keV carbon with a 1.5 cm range at 10 torr. As seen in Table 4, the average W-value for carbons in the energy interval 40 keV to 5.68 MeV is 40.15 eV/ip. Energy deposition is calculated using this average W-value, and control is then returned to NDOSE where the track-length estimate determined by subroutine LENGTH is used to calculate track-average LET.

If the original track-length estimate exceeds the tolerance interval, the analysis is aborted since this would constitute an impossible situation. Note that the tolerance interval used for stopper/starter separation can be decreased as the spatial resolution of the detector, and hence the accuracy of measured track lengths, increases.

Subroutine DEQUIV

Once the track's energy deposition and track length are determined, the algorithm's final task is to calculate the track's contribution to the total dose equivalent within subroutine DEQUIV. Since LET in methane is approximately equal to LET in water, DEQUIV performs a unit conversion of

the inferred LET in methane ($MeV \cdot cm^2/g$) to an equivalent LET in water ($keV/\mu m$). The resulting value is compared to the LET intervals of Table 2 to obtain a quality factor. Dose equivalent contribution in sieverts is then calculated by multiplying the energy deposition in joules by this quality factor and then dividing by the mass of the methane counting gas in kg.

CHAPTER 4

ALGORITHM TEST RESULTS AND CONCLUSIONS

Computer simulations can provide the basis for verification of dosimeter designs prior to construction and field testing. Simulations of the dosimeter response to any neutron field can be accomplished through detailed Monte Carlo transport calculations of the incident neutrons which produce recoil particles in the detector wall or gas cavity. Ideally, the digital algorithm presented in this thesis can be tested on calculations made from a neutron-transport code used in conjunction with ORNL's recoil-particle transport code. Since such a neutron-transport code was not yet available, a simplified Monte Carlo code was written to generate samples of recoils produced either at the inside surface of the detector wall or within the gas volume. ORNL's recoil-particle transport code was then used to transport these recoils through the methane gas cavity, followed by analysis of their ionization tracks by the algorithm. Three monoenergetic neutron-irradiation conditions were considered. The results of these sample runs are given in this chapter.

Testing Format

In this test simulation, the dosimeter was irradiated by monoenergetic neutron beams each perpendicularly incident on one face of the detector. The three energies considered

were 14 Mev, 200 keV, and 30 keV. The neutron interactions modeled were elastic scattering with hydrogen and carbon. Conservation of energy and momentum in a single collision dictate that the energy of the recoil particle, E_r, is given by

$$E_r = E_n \frac{4M_n M_r}{(M_n + M_r)^2} \cos^2\theta_r, \qquad (14)$$

where E_n is the incident neutron energy, θ_r is the polar angle of scatter for the recoil nucleus in the laboratory system, and M_n and M_r are the neutron and recoil masses, respectively (Tu85b). According to Equation 14, up to a 100% of the incident neutron energy can be transferred to hydrogen, while only 28.4% of the neutron energy can be transferred to carbon nuclei. Elastic scattering of neutrons with both nuclei (isotropic in the center-of-mass system) produces flat energy distributions (Kn79). The simplified neutron-transport code thus chose a random recoil energy uniformly between zero and the maximum energy transferred. The polar angle of scatter was then determined from Equation 14, while the azimuthal angle was chosen uniformly between 0 and 360 degrees.

Neutron interactions were assumed to occur either at the inside surface of the detector wall or within the gas cavity. Four populations of recoils were thus sampled for each incident neutron energy: protons produced at the detector wall, carbon ions produced at the detector wall, protons produced within the gas cavity, and carbon ions produced

within the gas cavity. Initial Y coordinates were set at 0 cm for all wall events, thus neglecting energy degradation from transport in the wall material. To insure that a large fraction of these recoils intersected the sensitive volume, starting X coordinates were chosen uniformly only between 2 and 12 cm. Z coordinates were chosen between 0 and 10 cm. The initial XYZ coordinates for recoils generated within the gas cavity were chosen between 2 and 12, 0 and 12, and 0 and 10 cm, respectively.

Results

Tables 15 through 24 given in the Appendix list the results of the algorithm testing procedure. Each table corresponds to a unique combination of neutron energy, recoil particle generated, and location of the initiating neutron interaction (detector wall or gas cavity). Tables for carbon ions produced in the wall by 200 and 30 keV neutrons are not listed since those recoil particles had insufficient energy to intersect the sensitive volume. For each recoil generated, the tables give the number of electrons produced, energy deposition, track length, LET, and dose equivalent contribution as determined by the Monte Carlo transport code (labeled MC) and as unfolded by the algorithm (labeled AL). Zero values for the Monte Carlo code indicated that the event did not intersect the sensitive volume, while zero values for the algorithm indicate that the analysis had been aborted for one of the reasons

discussed in Chapter 3. At the bottom of each table, sums and averages are given where appropriate.

Discussion and Assessment

The primary function of the algorithm is to unfold both energy deposition and dose equivalent to a reasonable degree of accuracy over a broad range of neutron energies. Tables 5 and 6 summarize attempts to unfold these quantities for the 14 MeV neutron runs listed in the Appendix. These tables indicate that, for proton events, average energy deposition is unfolded to within 1.0% of the Monte Carlo calculated average, while dose equivalent is unfolded to within 3.2% of its Monte Carlo average. Both average energy deposition and dose equivalent for carbon ions are unfolded to within 2.5% for wall events and to within 5.7% for gas events. At this neutron energy, all recoils were either crossers or starters, and thus these two classes of tracks were reasonably treated for both protons and carbon ions.

Tables 7 and 8 show that for protons generated by 200 keV neutrons, average energy deposition is unfolded to within three significant figures, while average dose equivalent is unfolded to within 17.4% for wall events and to within 14.2% for gas events. For carbon ions produced in the gas cavity, these average quantities are underestimated by the algorithm. Reported energy deposition is low by almost a factor of two, while reported dose equivalent is low by almost a factor of three. In a majority of these carbon events, the algorithm assumed the tracks were created

TABLE 5
Average energy deposition and dose equivalent produced by 14MeV neutrons having collisions at the inner surface of the detector wall

Protons	Monte Carlo	Algorithm
Energy Deposition (keV)	4.33	4.31
Dose Equivalent (Sv)	2.19E-10	2.26E-10
Carbon Ions		
Energy Deposition (keV)	589	604
Dose Equivalent (Sv)	2.16E-07	2.21E-07

TABLE 6
Average energy deposition and dose equivalent produced by 14 MeV neutrons having collisions within the gas cavity

Protons	Monte Carlo	Algorithm
Energy Deposition (keV)	7.04	6.97
Dose Equivalent (Sv)	1.13E-09	1.16E-09
Carbon Ions		
Energy Deposition (keV)	580	613
Dose Equivalent (Sv)	2.12E-07	2.24E-07

TABLE 7
Average energy deposition and dose equivalent produced by 200 keV neutrons having collisions at the inner surface of the detector wall

Protons	Monte Carlo	Algorithm
Energy Deposition (keV)	52.3	52.3
Dose Equivalent (Sv)	1.61E-08	1.33E-08

TABLE 8
Average energy deposition and dose equivalent produced by 200 keV neutrons having collisions within the gas cavity

Protons	Monte Carlo	Algorithm
Energy Deposition (keV)	38.5	38.5
Dose Equivalent (Sv)	1.20E-08	1.03E-08
Carbon Ions		
Energy Deposition (keV)	24.7	13.3
Dose Equivalent (Sv)	8.88E-09	3.28E-09

by protons, thus leading to underestimates of these quantities.

These misidentifications can be attributed to inaccurate estimates of electron numbers and track lengths. Using the algorithm values for the average number of electrons produced (397) and the average track length traversed (2.18 cm), one can calculate a mean mass stopping power of 0.62 x 10^3 MeV·cm^2/g. This value is below the proton Bragg peak, and thus carbon tracks are indistinguishable from proton tracks on the average. Using the corresponding values determined by the Monte Carlo code (426 electrons and 1.04 cm), one can calculate a mean mass stopping power of 1.40 x 10^3 MeV·cm^2/g. This value exceeds the proton Bragg peak such that, on the average, correct identification of particle type is still possible at this neutron energy. A detector with increased spatial resolution would therefore correct this problem through increased accuracy in track-length estimates given by the algorithm.

Table 9 shows energy deposition and dose equivalent averages for protons originating from wall events produced by 30 keV neutrons. Average energy deposition is unfolded to within 0.1%, yet reported dose equivalent is only 74.5% of the Monte Carlo value. The underestimate of dose equivalent can be traced to the algorithm's overestimate of average track length. One can calculate an average LET in water of 44.9 keV/μm using the Monte Carlo value 1.25 cm for average track length, and an average LET of 26.8 keV/μm using the algorithm's track-length estimate of 2.10 cm.

TABLE 9
Average energy deposition and dose equivalent produced by 30 keV neutrons having collisions at the inner surface of the detector wall

Protons	Monte Carlo	Algorithm
Energy Deposition (keV)	4.92	4.93
Dose Equivalent (Sv)	8.01E-10	5.97E-10

TABLE 10
Average energy deposition and dose equivalent produced by 30 keV neutrons having collisions within the gas cavity

Protons	Monte Carlo	Algorithm
Energy Deposition (keV)	12.0	11.8
Dose Equivalent (Sv)	2.47E-09	1.92E-09
Carbon Ions		
Energy Deposition (keV)	4.53	0.965
Dose Equivalent (Sv)	1.40E-09	9.17E-11

These LET values give a discrepancy for average proton quality factors of 8.28 versus 6.18.

Table 10 gives the results for proton and carbon recoils produced within the cavity by 30 keV neutrons. Average energy deposition for protons is unfolded to within 1.7% of the Monte Carlo value and dose equivalent to within 22.3%. The corresponding values for the carbon ions are greatly underestimated. In this case, the average mass stopping power of all carbon ions is below the proton Bragg peak, and particle-type identification is impossible. Using values for average electron production and average track length given by the Monte Carlo code, the average mass stopping power for all carbon events sampled is only 0.22 x 10^3 MeV·cm^2/g.

To better appreciate the effects of inaccurate carbon-track analyses to overall dose and dose equivalent averages, it is instructive to know, at each neutron energy, the percentage of all interactions within the detector wall and within the gas cavity which produce carbon ions versus the percentage which produce recoil protons. The physical data needed to determine these percentages are given in Tables 11 and 12. The resulting percentages for interactions within the wall and gas cavity are shown in Tables 13 and 14, respectively. Table 13 shows that only 9.1% of all interactions by 200 keV neutrons with methane produce carbon ions. At a neutron energy of 30 keV, only 6.3% of these interactions produce carbon ions.

TABLE 11
Atomic number density of hydrogen and carbon in methane at 10 torr and in polyethylene

	Target Material	
	Methane	Polyethylene
Atomic Number Density (cm^{-3})		
Hydrogen:	1.32×10^{18}	8.09×10^{22}
Carbon:	3.30×10^{17}	4.04×10^{22}

TABLE 12
Microscopic Cross Section for hydrogen and carbon at neutron energies 14 MeV, 200 keV, and 30 keV

	Interaction Nucleus	
	Hydrogen*	Carbon#
Microscopic Cross Section (10^{-24} cm^2)		
14 MeV:	0.7	1.5
200 keV:	10.0	4.0
30 keV:	17.4	4.7

* "Neutron Cross Sections," BNL 325, 2nd Ed., Suppl. No. 2, Brookhaven National Laboratory, Upton, NY (1964).

(Tu86)

TABLE 13
Percentage of interactions producing protons and carbon ions within methane gas at 10 torr

	Interaction Nuclei	
Neutron Energy	Hydrogen	Carbon
14 MeV	65.1%	34.9%
200 keV	90.9%	9.1%
30 keV	93.7%	6.3%

TABLE 14
Percentage of interactions producing protons and carbon ions within polyethylene

	Interaction Nuclei	
Neutron Energy	Hydrogen	Carbon
14 MeV	48.3%	51.7%
200 keV	83.3%	16.7%
30 keV	88.1%	11.9%

The relative contribution to dose equivalent by neutron interactions in the wall and those in the gas can only be assessed once recoils produced in the wall are degraded in energy by transport through the wall material. Under the simplistic conditions of the algorithm testing procedure, contributions from neutron interactions within the low-pressure gas-cavity are insignificant. However, when wall transport of recoils is later added, a neutron energy threshold will develop at which neither proton nor carbon recoils produced in the wall will reach the sensitive volume. Below that threshold, the response of the dosimeter will solely depend upon neutron interactions within the methane cavity.

From the discussions above, an overall assessment of the algorithm's performance would be favorable. The algorithm appears to unfold dose and dose equivalent accurately for both proton and carbon recoils produced by neutrons with energies in the tens of MeV. At energies of hundreds of keV, the carbon response is depressed. As shown in Figure 2, however, elastic scattering with heavy nuclei such as carbon contributes only slightly to overall tissue absorbed dose. Proton interactions remain the principal component to total tissue dose, and the algorithm's proton response is still accurate at these energies. At energies in the tens of keV, where conventional dosimeters perform poorly, the algorithm continues to accurately unfold proton dose and dose equivalent. The carbon response is greatly depressed at these energies.

The favorable performance of the algorithm was achieved under less-than-optimal conditions considering the physical limitations of the detector design discussed in Chapter 2. These limitations can cause, for individual tracks, large inaccuracies in unfolded parameters. The precision observed for average quantities is thus attributed to compensating errors. Individual worst-case situations are still of interest in improving the design of both the detector and the algorithm.

Table 17 given in the Appendix indicates two examples of how these detector limitations can adversely affect the unfolding of track lengths for individual events. The two runs marked with asterisks had track lengths largely underestimated by the algorithm. The corresponding LET and dose equivalent values are subsequently overestimated.

For the event marked by a single asterisk, the algorithm's track-length overestimate is attributed to the absence of a prompt triggering mechanism for events in the detector. As explained in Chapter 2, the resulting Z coordinates of collected electrons are made relative, not to the XY collection plane, but to the original Z coordinate of the first electron collected. Unable to discern whether the track was a starter exiting the upper XY face of the sensitive volume, or an inner at some lower height above the collection plane, the algorithm used a default decision and processed the track as an inner. The actual event was a 4.76 MeV proton created at XYZ coordinates 7.9, 2.7, and 5.1 cm, exiting the sensitive volume at 6.3, 6.4, and 10.0 cm.

The proton traveled 6.34 cm in the sensitive volume, deposited an initial 6.3 keV of kinetic energy, and produced 215 ion pairs. The detector measured 209 electrons, and the algorithm estimated that 6.27 keV was deposited. Since the algorithm assumed the track was an inner, 1.72 cm was given as the track-length estimate, where 1.72 cm is the range of a 6.27 keV proton in methane at 10 torr.

Two solutions are possible to correct such inaccuracies. One solution would establish an energy cutoff such that the algorithm will process all questionable tracks as starters for energy depositions greater than this value, and as inners for energy depositions below this value. This solution will only work for proton events; energy deposition for carbon tracks is found only after the type of track (starter or inner) is known. A second solution, good for proton tracks only, would have the algorithm avoid using a range curve to estimate track length for proton inners. The algorithm would then treat all proton tracks equally. (Range curves were used in an attempt to overcome the effects of course spatial resolution in measuring track lengths.)

For the event marked by two asterisks, diffusion effects altered the original pattern of triggered cells such that subroutine SEARCH incorrectly chose the cells thought to contain the true track endpoints within the sensitive volume. The track-length estimate given by subroutine LENGTH was subsequently in error. The solution in this case

would be a detector exhibiting little or no diffusion effects during collection.

Certainly, a detector designed to overcome all the physical limitations discussed in Chapter 2 would greatly improve the unfolding process. Given the output of such a detector, one would expect an enhanced performance by the algorithm without any major modifications.

CHAPTER 5

SUMMARY AND RECOMMENDATIONS

This thesis provides an essential step in the development of ORNL's digital approach to neutron dosimetry. Previous work at ORNL resulted in a Monte Carlo computer code which simulates the creation of subexcitation electrons by recoil nuclei within subvolumes (cells) of a hydrocarbon-lined time-projection chamber. The detector design calls for a 1000 cell partitioning of its sensitive volume producing a 1000 integer array giving the integral number of subexcitation electrons created within each cell. This simulation code was then used to develop the computer algorithm presented in this thesis. The algorithm estimates neutron absorbed dose, LET, and dose equivalent for each registered event given the detector's integer array.

The algorithm begins by estimating the event's track length within the sensitive volume. This is accomplished by measuring the line segment connecting the spatial centers of the two cells most likely to contain the track's endpoints. The integer array is then summed to estimate the total number of electrons created by the track segment. Protons exhibit a constant W-value of 30 eV/ip within the methane detection cavity; the algorithm therefore uses this W-value along with its estimates of track length and electron production to calculate an average mass stopping power for

the track assuming it was created by a proton. The algorithm then compares this result to the Bragg peak of the proton mass stopping power curve. If the result exceeds this peak value, the track is labeled a carbon; if not, the track is labeled a proton.

Proton energy deposition is calculated using W=30 eV/ip. The W-value of carbon ions in methane is energy dependent; energy deposition by carbon tracks is therefore determined only after an average W-value for such tracks is found. The procedure for finding this average W-value differs depending upon whether the track is a crosser, inner, stopper, or starter. LET and dose equivalent are determined for both particle types using final estimates of track length and energy deposition.

To assess the accuracy of the algorithm in unfolding the quantities absorbed dose and dose equivalent, a variety of recoils produced by 14 MeV, 200 keV, and 30 keV neutrons were transported by the detector simulation code. The output of each run was then analyzed by the algorithm and its unfolded quantities were subsequently compared to those calculated by the simulation code.

The results indicate that the algorithm performs accurately for both proton and carbon events at neutron energies in the tens of MeV. Proton-track analysis continues to be accurate down to neutron energies in the tens of keV. At these energies, algorithm accuracy becomes increasingly dependent upon the detector's spatial resolution. Discrimination of carbon events becomes impossible at

neutron energies below 200 keV. These tracks are thus analyzed as proton events causing underestimates of absorbed dose. At these lower energies, however, carbon events become less frequent and thus their contribution to total absorbed dose and dose equivalent decreases.

Four essential steps remain in the development of the digital approach. First, fine-tuning of the algorithm should be accomplished by reviewing each run listed in the tables of the Appendix. Large overestimates or underestimates of either energy deposition or track length should be traced either to limitations of the detector design, limitations of the algorithm methodology, or flaws in the algorithm logic. If errors are due to the latter, the algorithm code should be corrected accordingly.

The second step needed is a detailed simulation of the dosimeter's response to a variety of neutron energies and incident directions in order to verify the entire dosimeter design. Instead of comparing average quantities as was done in this thesis, a comparison should be made between distributions of energy deposition, track length, and LET calculated by the Monte Carlo recoil-transport code and cooresponding distributions unfolded by the algorithm. Third, a prototype detector should be constructed to prove the feasibility of digital pulse collection, provided development funding is available. Fourth, this prototype detector and the algorithm should be field tested in a well-known neutron field such as that produced at Oak Ridge's DOSAR facility.

APPENDIX

RESULTS OF TESTING PROCEDURE

TABLE 15
Test results for 14 MeV neutrons producing protons at the inner wall surface

#Electrons		Energy Deposited (eV)		Tracklength (cm)		LET (Mev*cm2/g)		Dose Equiv (Sv)	
MC	AL	MC	AL	MC	AL	MC	AL	MC	AL
182	192	5.53E+03	5.76E+03	10.41	7.80	6.07E+01	8.43E+01	1.52E-10	2.97E-10
58	59	1.95E+03	1.77E+03	5.82	1.41	3.82E+01	1.43E+02	5.35E-11	9.13E-11
70	85	2.49E+03	2.55E+03	7.65	4.37	3.72E+01	6.67E+01	6.84E-11	7.00E-11
52	49	1.51E+03	1.47E+03	2.07	3.46	8.36E+01	4.85E+01	7.80E-11	4.03E-11
134	146	3.96E+03	4.38E+03	10.36	10.94	4.37E+01	4.57E+01	1.09E-10	1.20E-10
49	81	1.34E+03	2.43E+03	0.72	3.16	2.12E+02	8.78E+01	1.09E-10	1.25E-10
197	182	5.68E+03	5.46E+03	6.34	6.64	1.02E+02	9.38E+01	2.93E-10	2.82E-10
141	167	4.41E+03	5.01E+03	11.57	11.65	4.36E+01	4.91E+01	1.21E-10	1.38E-10
3	0	6.27E+01	0.00E+00	0.38	0.00	1.88E+01	0.00E+00	1.15E-12	0.00E+00
217	232	6.42E+03	6.96E+03	11.18	9.02	6.56E+01	8.82E+01	1.76E-10	3.59E-10
54	54	1.90E+03	1.62E+03	6.28	4.77	3.46E+01	3.88E+01	3.48E-11	4.45E-11
107	108	3.20E+03	3.24E+03	3.60	5.20	1.02E+02	7.12E+01	1.65E-10	1.67E-10
361	348	1.10E+04	1.04E+04	3.85	7.65	3.25E+02	1.56E+02	1.24E-09	8.54E-10
176	178	5.51E+03	5.34E+03	9.78	7.87	6.43E+01	7.75E+01	1.51E-10	2.76E-10
22	0	6.93E+02	0.00E+00	0.78	0.00	1.01E+02	0.00E+00	3.57E-11	0.00E+00
125	121	3.62E+03	3.63E+03	10.92	9.32	3.79E+01	4.45E+01	9.93E-11	9.96E-11
207	205	6.54E+03	6.15E+03	10.29	9.94	7.26E+01	7.07E+01	3.38E-10	3.17E-10
549	530	1.59E+04	1.59E+04	6.97	6.90	2.60E+02	2.63E+02	1.79E-09	1.80E-09
374	384	1.12E+04	1.15E+04	13.94	11.44	9.20E+01	1.15E+02	5.79E-10	5.94E-10
109	110	3.46E+03	3.30E+03	10.34	10.48	3.82E+01	3.60E+01	9.49E-11	9.06E-11
201	208	6.19E+03	6.24E+03	11.20	8.23	6.31E+01	8.66E+01	1.70E-10	3.22E-10
199	194	5.74E+03	5.82E+03	10.43	6.41	6.28E+01	1.04E+02	1.57E-10	3.00E-10
145	151	4.37E+03	4.53E+03	11.40	11.49	4.38E+01	4.50E+01	1.20E-10	1.24E-10
80	90	2.77E+03	2.70E+03	10.47	8.76	3.02E+01	3.52E+01	5.06E-11	7.41E-11
212	214	6.18E+03	6.42E+03	11.18	7.19	6.31E+01	1.02E+02	1.70E-10	3.31E-10
145	156	4.46E+03	4.68E+03	11.43	11.00	4.46E+01	4.86E+01	1.23E-10	1.28E-10
58	58	1.83E+03	1.74E+03	1.57	2.12	1.33E+02	9.37E+01	9.45E-11	8.98E-11
86	87	2.48E+03	2.61E+03	3.04	4.51	9.32E+01	6.61E+01	1.28E-10	7.16E-11
60	0	1.82E+03	0.00E+00	5.93	0.00	3.50E+01	0.00E+00	4.99E-11	0.00E+00
124	121	3.68E+03	3.63E+03	7.45	7.39	5.63E+01	5.61E+01	1.01E-10	9.96E-11
173	175	5.17E+03	5.25E+03	6.38	6.06	9.25E+01	9.90E+01	2.67E-10	2.71E-10
147	124	4.39E+03	3.72E+03	4.54	5.30	1.11E+02	8.01E+01	2.27E-10	1.92E-10
290	293	9.01E+03	8.79E+03	5.83	7.27	1.77E+02	1.38E+02	7.37E-10	4.53E-10
90	102	2.66E+03	3.06E+03	2.77	4.29	1.10E+02	8.15E+01	1.37E-10	1.58E-10
123	142	3.69E+03	4.26E+03	6.37	7.18	6.62E+01	6.77E+01	1.01E-10	1.17E-10
185	245	5.48E+03	7.35E+03	1.15	6.36	5.44E+02	1.32E+02	1.03E-09	3.79E-10
33	39	8.36E+02	1.17E+03	1.58	1.50	6.03E+01	8.91E+01	2.29E-11	6.04E-11
240	240	6.69E+03	7.20E+03	6.02	5.47	1.27E+02	1.50E+02	3.45E-10	5.89E-10
366	363	1.05E+04	1.09E+04	7.86	9.04	1.52E+02	1.38E+02	8.57E-10	5.62E-10
19	0	7.21E+02	0.00E+00	1.26	0.00	6.54E+01	0.00E+00	1.98E-11	0.00E+00
20	20	6.15E+02	6.00E+02	1.71	2.12	4.11E+01	3.23E+01	1.69E-11	1.10E-11

TABLE 15 (continued)

#Electrons		Energy Deposited (eV)		Tracklength (cm)		LET (Mev*cm2/g)		Dose Equiv (Sv)	
MC	AL	MC	AL	MC	AL	MC	AL	MC	AL
48	55	1.52E+03	1.65E+03	2.82	2.60	6.14E+01	7.25E+01	4.16E-11	8.51E-11
109	120	3.56E+03	3.60E+03	10.64	6.94	3.82E+01	5.93E+01	9.77E-11	9.88E-11
218	185	6.29E+03	5.55E+03	10.47	10.12	6.86E+01	6.26E+01	1.73E-10	1.52E-10
66	66	2.11E+03	1.98E+03	3.66	6.24	6.58E+01	3.63E+01	5.80E-11	5.43E-11
62	58	1.86E+03	1.74E+03	5.88	2.50	3.62E+01	7.95E+01	5.11E-11	8.98E-11
102	105	3.07E+03	3.15E+03	7.28	5.50	4.82E+01	6.54E+01	8.43E-11	8.64E-11
90	100	2.91E+03	3.00E+03	10.43	9.08	3.18E+01	3.77E+01	5.32E-11	8.23E-11
19	0	6.25E+02	0.00E+00	1.22	0.00	5.87E+01	0.00E+00	1.72E-11	0.00E+00
265	274	7.91E+03	8.22E+03	5.81	9.22	1.55E+02	1.02E+02	6.46E-10	4.24E-10
366	324	1.03E+04	9.72E+03	4.89	9.92	2.41E+02	1.12E+02	8.44E-10	5.01E-10
90	144	3.06E+03	4.32E+03	1.22	4.00	2.87E+02	1.23E+02	3.46E-10	2.23E-10
284	283	8.15E+03	8.49E+03	10.70	11.20	8.70E+01	8.66E+01	4.20E-10	4.38E-10
50	52	1.66E+03	1.56E+03	6.68	6.59	2.84E+01	2.70E+01	3.04E-11	2.85E-11
164	176	5.25E+03	5.28E+03	10.62	1.53	5.64E+01	3.94E+02	1.44E-10	8.00E-10
110	130	3.38E+03	3.90E+03	10.02	7.58	3.85E+01	5.88E+01	9.27E-11	1.07E-10
92	95	2.93E+03	2.85E+03	8.12	1.00	4.12E+01	3.24E+02	8.03E-11	3.22E-10
144	156	4.22E+03	4.68E+03	8.70	1.41	5.53E+01	3.79E+02	1.16E-10	7.09E-10
347	331	1.00E+04	9.93E+03	12.92	13.24	8.87E+01	8.56E+01	5.18E-10	5.12E-10
68	76	2.08E+03	2.28E+03	7.21	0.86	3.29E+01	3.03E+02	3.80E-11	2.58E-10
134	133	4.20E+03	3.99E+03	2.00	7.26	2.40E+02	6.27E+01	3.43E-10	1.10E-10
295	283	8.45E+03	8.49E+03	12.15	10.89	7.94E+01	8.90E+01	4.36E-10	4.38E-10
73	76	2.36E+03	2.28E+03	7.21	7.18	3.74E+01	3.63E+01	6.48E-11	6.26E-11
15	0	3.98E+02	0.00E+00	1.05	0.00	4.34E+01	0.00E+00	1.09E-11	0.00E+00
300	318	9.47E+03	9.54E+03	8.41	8.29	1.29E+02	1.31E+02	4.89E-10	4.92E-10
132	131	4.22E+03	3.93E+03	11.30	11.21	4.26E+01	4.00E+01	1.16E-10	1.08E-10
173	176	5.31E+03	5.28E+03	7.20	6.73	8.41E+01	8.96E+01	2.74E-10	2.72E-10
34	0	1.07E+03	0.00E+00	1.54	0.00	7.94E+01	0.00E+00	5.53E-11	0.00E+00
81	85	2.77E+03	2.55E+03	10.08	8.63	3.14E+01	3.37E+01	5.07E-11	4.67E-11
217	232	5.80E+03	6.96E+03	10.10	10.12	6.56E+01	7.85E+01	1.59E-10	3.59E-10
53	49	1.48E+03	1.47E+03	0.90	1.41	1.87E+02	1.19E+02	1.21E-10	7.58E-11
121	120	3.79E+03	3.60E+03	5.43	6.06	7.99E+01	6.79E+01	1.96E-10	9.88E-11
74	73	2.26E+03	2.19E+03	8.01	9.62	3.22E+01	2.60E+01	4.14E-11	4.01E-11
22	32	8.29E+02	9.60E+02	0.97	1.50	9.71E+01	7.31E+01	4.28E-11	4.95E-11
115	108	3.17E+03	3.24E+03	3.04	3.91	1.19E+02	9.46E+01	1.64E-10	1.67E-10
481	487	1.37E+04	1.46E+04	5.28	8.32	2.96E+02	2.01E+02	1.55E-09	1.20E-09
108	117	3.44E+03	3.51E+03	5.83	5.09	6.73E+01	7.88E+01	9.43E-11	1.81E-10
324	327	9.74E+03	9.81E+03	7.87	9.19	1.41E+02	1.22E+02	5.03E-10	5.06E-10
229	230	7.12E+03	6.90E+03	12.17	11.44	6.68E+01	6.89E+01	1.95E-10	1.89E-10
79	98	2.84E+03	2.94E+03	5.50	4.37	5.90E+01	7.69E+01	7.80E-11	1.52E-10
111	129	3.57E+03	3.87E+03	10.07	7.71	4.05E+01	5.74E+01	9.80E-11	1.06E-10
176	167	5.26E+03	5.01E+03	10.34	7.80	5.80E+01	7.33E+01	1.44E-10	2.58E-10

TABLE 15 (continued)

	#Electrons		Energy Deposited (eV)		Tracklength (cm)		LET (Mev*cm2/g)		Dose Equiv (Sv)	
	MC	AL	MC	AL	MC	AL	MC	AL	MC	AL
	44	42	1.29E+03	1.26E+03	2.95	2.80	5.00E+01	5.15E+01	3.55E-11	3.46E-11
	111	111	3.46E+03	3.33E+03	3.84	4.97	1.03E+02	7.64E+01	1.79E-10	1.72E-10
	44	54	1.27E+03	1.62E+03	1.05	3.00	1.39E+02	6.17E+01	6.57E-11	4.45E-11
	317	340	1.00E+04	1.02E+04	11.63	9.65	9.85E+01	1.21E+02	5.17E-10	5.26E-10
	237	242	7.62E+03	7.26E+03	13.08	9.76	6.65E+01	8.49E+01	2.09E-10	3.75E-10
	67	66	2.26E+03	1.98E+03	5.43	3.87	4.74E+01	5.84E+01	6.19E-11	5.43E-11
	22	0	8.63E+02	0.00E+00	3.36	0.00	2.94E+01	0.00E+00	1.58E-11	0.00E+00
	103	99	3.43E+03	2.97E+03	3.09	3.91	1.27E+02	8.67E+01	1.77E-10	1.53E-10
	143	161	4.35E+03	4.83E+03	7.04	5.47	7.06E+01	1.01E+02	2.25E-10	2.49E-10
	356	375	1.07E+04	1.13E+04	11.10	12.47	1.10E+02	1.03E+02	5.51E-10	5.80E-10
	178	188	5.29E+03	5.64E+03	10.37	7.87	5.83E+01	8.18E+01	1.45E-10	2.91E-10
	5	0	2.86E+02	0.00E+00	1.46	0.00	2.23E+01	0.00E+00	5.24E-12	0.00E+00
	89	79	3.00E+03	2.37E+03	3.76	5.11	9.11E+01	5.30E+01	1.55E-10	6.50E-11
	276	286	8.23E+03	8.58E+03	8.07	7.96	1.16E+02	1.23E+02	4.24E-10	4.43E-10
	20	0	6.90E+02	0.00E+00	2.32	0.00	3.40E+01	0.00E+00	1.26E-11	0.00E+00
	19	0	6.73E+02	0.00E+00	2.09	0.00	3.68E+01	0.00E+00	1.85E-11	0.00E+00
	76	0	2.52E+03	0.00E+00	10.26	0.00	2.81E+01	0.00E+00	4.62E-11	0.00E+00
	109	104	3.34E+03	3.12E+03	10.11	8.54	3.77E+01	4.17E+01	9.16E-11	8.56E-11
	112	117	3.41E+03	3.51E+03	10.11	6.50	3.85E+01	6.17E+01	9.34E-11	9.63E-11
	32	0	1.09E+03	0.00E+00	2.92	0.00	4.28E+01	0.00E+00	3.00E-11	0.00E+00
	76	85	2.59E+03	2.55E+03	10.45	9.02	2.83E+01	3.23E+01	4.74E-11	4.67E-11
	454	470	1.29E+04	1.41E+04	10.05	10.25	1.46E+02	1.57E+02	6.64E-10	1.15E-09
	137	126	4.38E+03	3.78E+03	5.17	4.68	9.68E+01	9.23E+01	2.26E-10	1.95E-10
	124	130	3.75E+03	3.90E+03	5.89	6.70	7.27E+01	6.65E+01	1.94E-10	1.07E-10
	136	145	3.88E+03	4.35E+03	10.88	10.54	4.08E+01	4.71E+01	1.07E-10	1.19E-10
	192	193	5.86E+03	5.79E+03	10.87	11.00	6.16E+01	6.01E+01	1.61E-10	1.59E-10
	112	121	3.30E+03	3.63E+03	3.54	4.51	1.06E+02	9.20E+01	1.70E-10	1.87E-10
	16	17	5.14E+02	5.10E+02	0.48	1.00	1.21E+02	5.82E+01	2.65E-11	1.40E-11
	109	111	3.43E+03	3.33E+03	4.95	4.81	7.90E+01	7.91E+01	1.77E-10	1.72E-10
	152	164	4.60E+03	4.92E+03	10.63	9.14	4.94E+01	6.15E+01	1.26E-10	1.35E-10
	39	0	1.27E+03	0.00E+00	2.03	0.00	7.11E+01	0.00E+00	6.53E-11	0.00E+00
	201	209	5.90E+03	6.27E+03	9.39	8.89	7.17E+01	8.06E+01	3.04E-10	3.23E-10
sum:			4.94E+05	4.92E+05					2.50E-08	2.58E-08
avg:	143	144	4.33E+03	4.31E+03	6.73	5.99	8.68E+01	8.06E+01	2.19E-10	2.26E-10

TABLE 16
Test results for 14 MeV neutrons producing carbon ions at the inner wall surface

	#Electrons		Energy Deposited (eV)		Tracklength (cm)		LET (Mev*cm2/g)		Dose Equiv (Sv)	
	MC	AL	MC	AL	MC	AL	MC	AL	MC	AL
	30724	30690	1.06E+06	1.08E+06	9.93	10.54	1.22E+04	1.17E+04	3.87E-07	3.95E-07
	22952	22987	8.05E+05	8.08E+05	7.67	10.14	1.20E+04	9.10E+03	2.94E-07	2.96E-07
	16209	16235	5.82E+05	5.71E+05	5.90	8.71	1.13E+04	7.48E+03	2.13E-07	2.09E-07
	11902	11798	4.35E+05	4.74E+05	4.55	8.33	1.09E+04	6.50E+03	1.59E-07	1.73E-07
	13494	13311	4.87E+05	5.34E+05	5.11	8.33	1.09E+04	7.33E+03	1.78E-07	1.96E-07
	36109	36187	1.27E+06	1.27E+06	12.20	14.53	1.19E+04	1.00E+04	4.66E-07	4.65E-07
	3985	4134	1.55E+05	1.45E+05	2.03	4.90	8.71E+03	3.39E+03	5.66E-08	5.32E-08
	12962	12968	4.54E+05	5.21E+05	4.36	4.38	1.19E+04	1.36E+04	1.66E-07	1.91E-07
	16019	16064	5.77E+05	5.65E+05	6.01	8.80	1.10E+04	7.33E+03	2.11E-07	2.07E-07
	1947	2118	6.86E+04	7.45E+04	0.67	3.00	1.16E+04	2.83E+03	2.51E-08	2.72E-08
sum:			5.89E+06	6.04E+06					2.16E-06	2.21E-06
avg:	16630	16649	5.89E+05	6.04E+05	5.85	8.17	1.12E+04	7.92E+03	2.16E-07	2.21E-07

TABLE 17
Test results for 14 MeV neutrons producing protons within the gas cavity

	#Electrons		Energy Deposited (eV)		Tracklength (cm)		LET (Mev*cm2/g)		Dose Equiv (Sv)		
	MC	AL	MC	AL	MC	AL	MC	AL	MC	AL	
	102	89	3.45E+03	2.67E+03	3.54	4.50	1.11E+02	6.78E+01	1.78E-10	7.33E-11	
	10	19	3.13E+02	5.70E+02	0.91	1.00	3.95E+01	6.51E+01	8.59E-12	1.56E-11	
	85	96	2.64E+03	2.88E+03	7.10	7.76	4.24E+01	4.24E+01	7.24E-11	7.90E-11	
	4	0	2.71E+02	0.00E+00	0.38	0.00	3.53E+01	0.00E+00	7.44E-12	0.00E+00	
	78	77	2.15E+03	2.31E+03	2.61	3.06	9.41E+01	8.62E+01	1.11E-10	1.19E-10	
	205	211	5.95E+03	6.33E+03	11.15	9.56	6.09E+01	7.56E+01	1.63E-10	3.27E-10	
	23	30	6.84E+02	9.00E+02	2.03	1.41	3.84E+01	7.27E+01	1.88E-11	4.64E-11	
	399	403	1.18E+04	1.21E+04	11.38	2.65	1.19E+02	5.21E+02	6.10E-10	2.28E-09	
	84	93	2.80E+03	2.79E+03	5.75	4.68	5.57E+01	6.81E+01	7.69E-11	7.66E-11	
	122	118	3.57E+03	3.54E+03	4.40	6.25	9.26E+01	6.46E+01	1.84E-10	9.71E-11	
	92	95	2.81E+03	2.85E+03	7.01	1.00	4.58E+01	3.24E+02	7.71E-11	3.22E-10	**
	440	432	1.35E+04	1.30E+04	8.36	8.96	1.84E+02	1.65E+02	1.10E-09	1.06E-09	
	195	203	5.56E+03	6.09E+03	10.63	8.83	5.97E+01	7.88E+01	1.53E-10	3.14E-10	
	13	0	3.31E+02	0.00E+00	0.31	0.00	1.21E+02	0.00E+00	1.71E-11	0.00E+00	
	562	566	1.72E+04	1.70E+04	10.70	12.22	1.83E+02	1.59E+02	1.40E-09	1.39E-09	
	36	0	1.20E+03	0.00E+00	3.43	0.00	4.01E+01	0.00E+00	3.30E-11	0.00E+00	
	46	47	1.42E+03	1.41E+03	2.06	2.24	7.85E+01	7.20E+01	7.31E-11	7.27E-11	
	215	209	6.25E+03	6.27E+03	6.34	1.72	1.13E+02	4.17E+02	3.23E-10	9.50E-10	*
	28	29	9.05E+02	8.70E+02	2.28	1.50	4.53E+01	6.62E+01	2.48E-11	2.39E-11	
	69	69	1.95E+03	2.07E+03	2.14	0.80	1.04E+02	2.94E+02	1.00E-10	2.34E-10	
	2656	2656	7.83E+04	7.97E+04	7.87	9.46	1.14E+03	9.62E+02	2.51E-08	2.17E-08	
	23	0	7.88E+02	0.00E+00	1.39	0.00	6.45E+01	0.00E+00	2.16E-11	0.00E+00	
	122	116	3.68E+03	3.48E+03	5.03	5.09	8.34E+01	7.81E+01	1.90E-10	1.80E-10	
	12	0	4.23E+02	0.00E+00	1.22	0.00	3.96E+01	0.00E+00	1.16E-11	0.00E+00	
	0	0	0.00E+00	0.00E+00	0.14	0.00	0.00E+00	0.00E+00	0.00E+00	0.00E+00	
	462	461	1.36E+04	1.38E+04	7.40	2.90	2.10E+02	5.45E+02	1.11E-09	2.61E-09	
	671	680	2.09E+04	2.04E+04	8.61	8.83	2.77E+02	2.64E+02	2.36E-09	2.31E-09	
	11	0	4.01E+02	0.00E+00	1.07	0.00	4.27E+01	0.00E+00	1.10E-11	0.00E+00	
	70	78	2.24E+03	2.34E+03	8.54	0.88	3.00E+01	3.05E+02	4.10E-11	2.65E-10	
	193	194	6.06E+03	5.82E+03	5.62	5.73	1.23E+02	1.16E+02	3.13E-10	3.00E-10	
sum:			2.11E+05	2.09E+05					3.39E-08	3.49E-08	
avg:	234	232	7.04E+03	6.97E+03	5.00	3.70	1.22E+02	1.64E+02	1.13E-09	1.16E-09	

* See Page 85
** See Page 85

TABLE 18
Test results for 14 MeV neutrons producing carbon ions within the gas cavity

	#Electrons		Energy Deposited (eV)		Tracklength (cm)		LET (Mev*cm2/g)		Dose Equiv (Sv)	
	MC	AL	MC	AL	MC	AL	MC	AL	MC	AL
	2074	2123	7.14E+04	7.46E+04	0.67	2.00	1.21E+04	4.26E+03	2.61E-08	2.73E-08
	9605	9650	3.38E+05	3.87E+05	3.21	4.95	1.20E+04	8.94E+03	1.24E-07	1.42E-07
	35865	35879	1.25E+06	1.26E+06	11.69	13.56	1.22E+04	1.06E+04	4.57E-07	4.61E-07
	33373	32480	1.20E+06	1.14E+06	12.04	14.58	1.13E+04	8.94E+03	4.37E-07	4.18E-07
	22865	22765	7.97E+05	9.14E+05	7.61	8.69	1.20E+04	1.20E+04	2.92E-07	3.34E-07
	3933	4005	1.37E+05	1.41E+05	1.30	3.00	1.20E+04	5.36E+03	5.02E-08	5.15E-08
	21274	21290	7.83E+05	8.55E+05	8.94	9.83	9.99E+03	9.93E+03	2.86E-07	3.13E-07
	9269	9232	3.18E+05	3.71E+05	2.96	6.07	1.23E+04	6.97E+03	1.17E-07	1.36E-07
	24130	22825	8.48E+05	9.16E+05	8.08	9.27	1.20E+04	1.13E+04	3.10E-07	3.35E-07
	1911	1893	6.44E+04	6.65E+04	0.62	1.41	1.19E+04	5.37E+03	2.36E-08	2.43E-08
sum:			5.80E+06	6.13E+06					2.12E-06	2.24E-06
avg:	16430	16214	5.80E+05	6.13E+05	5.71	7.34	1.18E+04	8.37E+03	2.12E-07	2.24E-07

TABLE 19
Test results for 2ØØ keV neutrons producing protons at the inner wall surface

#Electrons		Energy Deposited (eV)		Tracklength (cm)		LET (Mev*cm2/g)		Dose Equiv (Sv)	
MC	AL	MC	AL	MC	AL	MC	AL	MC	AL
0	55	0.00E+00	1.65E+03	0.00	3.00	0.00E+00	6.28E+01	0.00E+00	4.53E-11
3609	3634	1.09E+05	1.09E+05	10.92	11.92	1.14E+03	1.05E+03	3.49E-08	3.49E-08
3476	3496	1.04E+05	1.05E+05	10.60	11.65	1.13E+03	1.03E+03	3.34E-08	3.36E-08
37	0	8.96E+02	0.00E+00	0.15	0.00	6.79E+02	0.00E+00	1.93E-10	0.00E+00
1115	1118	3.43E+04	3.35E+04	3.74	5.53	1.05E+03	6.93E+02	1.10E-08	7.24E-09
3117	3133	9.41E+04	9.40E+04	10.03	10.24	1.07E+03	1.05E+03	3.01E-08	3.01E-08
592	584	1.79E+04	1.75E+04	3.47	5.73	5.90E+02	3.49E+02	3.37E-09	
1486	1466	4.48E+04	4.40E+04	5.61	7.94	9.12E+02	6.33E+02	1.22E-08	9.49E-09
1364	1389	4.17E+04	4.17E+04	4.06	6.59	1.17E+03	7.22E+02	1.34E-08	
322	327	9.74E+03	9.81E+03	1.35	3.16	8.26E+02	3.54E+02	2.42E-09	
83	139	2.94E+03	4.17E+03	1.11	3.00	3.04E+02	1.59E+02	3.32E-10	3.41E-10
3313	3338	9.96E+04	1.00E+05	10.29	10.77	1.11E+03	1.06E+03	3.19E-08	3.21E-08
749	747	2.27E+04	2.24E+04	2.23	6.55	1.16E+03	3.91E+02	7.26E-09	3.39E-09
649	683	1.99E+04	2.05E+04	3.62	7.18	6.28E+02	3.26E+02	4.29E-09	
2420	2447	7.39E+04	7.34E+04	9.26	10.05	9.11E+02	8.34E+02	2.01E-08	1.83E-08
1116	1135	3.38E+04	3.41E+04	4.31	5.15	8.96E+02	7.54E+02	9.22E-09	8.47E-09
3208	3240	9.60E+04	9.72E+04	10.01	10.06	1.09E+03	1.10E+03	3.07E-08	3.11E-08
728	736	2.20E+04	2.21E+04	2.16	2.60	1.16E+03	9.70E+02	7.03E-09	6.02E-09
2449	2450	7.34E+04	7.35E+04	7.09	7.38	1.18E+03	1.14E+03	2.35E-08	2.35E-08
668	692	2.05E+04	2.08E+04	3.91	8.22	5.98E+02	2.89E+02	3.86E-09	2.35E-09
932	965	2.77E+04	2.90E+04	2.75	3.69	1.15E+03	8.96E+02	8.88E-09	7.89E-09
1047	1059	3.18E+04	3.18E+04	3.41	5.03	1.06E+03	7.21E+02	1.02E-08	6.86E-09
24	86	7.19E+02	2.58E+03	0.30	2.24	2.74E+02	1.32E+02	8.13E-11	1.33E-10
1564	1577	4.68E+04	4.73E+04	4.75	8.43	1.13E+03	6.41E+02	1.50E-08	
1921	1925	5.73E+04	5.78E+04	5.62	5.74	1.16E+03	1.15E+03	1.83E-08	1.85E-08
188	229	6.08E+03	6.87E+03	0.60	3.16	1.16E+03	2.48E+02	1.95E-09	5.62E-10
2794	2804	8.53E+04	8.41E+04	8.86	10.08	1.10E+03	9.53E+02	2.73E-08	2.29E-08
2455	2419	7.37E+04	7.26E+04	9.16	12.58	9.19E+02	6.59E+02	2.01E-08	1.57E-08
348	328	1.07E+04	9.84E+03	1.09	2.00	1.13E+03	5.62E+02	3.43E-09	1.85E-09
1902	1845	5.75E+04	5.54E+04	7.11	11.92	9.24E+02	5.30E+02	1.57E-08	
1942	1910	5.88E+04	5.73E+04	5.74	8.29	1.17E+03	7.90E+02	1.88E-08	1.43E-08
3649	3659	1.09E+05	1.10E+05	10.88	12.07	1.14E+03	1.04E+03	3.48E-08	3.51E-08
3640	3644	1.09E+05	1.09E+05	10.91	12.07	1.14E+03	1.03E+03	3.50E-08	3.50E-08
3651	3646	1.09E+05	1.09E+05	10.94	11.92	1.14E+03	1.05E+03	3.50E-08	3.50E-08
755	740	2.32E+04	2.22E+04	2.96	6.18	8.92E+02	4.10E+02	6.31E-09	3.36E-09
1156	1161	3.53E+04	3.48E+04	3.49	5.66	1.16E+03	7.03E+02	1.13E-08	7.52E-09
3643	3631	1.09E+05	1.09E+05	10.82	11.92	1.15E+03	1.04E+03	3.48E-08	3.49E-08
3653	3585	1.10E+05	1.08E+05	11.46	12.72	1.09E+03	9.66E+02	3.51E-08	2.93E-08
13	85	2.40E+02	2.55E+03	0.05	3.35	5.90E+02	8.68E+01	4.53E-11	1.32E-10
1980	1957	5.94E+04	5.87E+04	6.00	9.98	1.13E+03	6.72E+02	1.90E-08	1.27E-08
2847	2876	8.61E+04	8.63E+04	8.44	8.64	1.17E+03	1.14E+03	2.76E-08	2.76E-08
189	214	5.59E+03	6.42E+03	0.89	4.74	7.20E+02	1.55E+02	1.21E-09	5.25E-10

TABLE 19 (continued)

	#Electrons		Energy Deposited (eV)		Tracklength (cm)		LET (Mev*cm2/g)		Dose Equiv (Sv)	
	MC	AL	MC	AL	MC	AL	MC	AL	MC	AL
	3407	3406	1.04E+05	1.02E+05	10.45	10.94	1.13E+03	1.07E+03	3.32E-08	3.27E-08
	2239	2231	6.66E+04	6.69E+04	8.33	10.71	9.12E+02	7.14E+02	1.81E-08	1.45E-08
	1057	1054	3.17E+04	3.16E+04	4.97	7.18	7.29E+02	5.03E+02	6.84E-09	5.96E-09
	1955	1975	6.03E+04	5.93E+04	8.37	11.13	8.23E+02	6.08E+02	1.50E-08	1.12E-08
	2083	2044	6.08E+04	6.13E+04	5.73	8.48	1.21E+03	8.26E+02	1.95E-08	1.53E-08
	668	646	1.98E+04	1.94E+04	2.26	6.64	1.00E+03	3.33E+02	6.35E-09	
	1791	1813	5.34E+04	5.44E+04	5.38	7.13	1.14E+03	8.71E+02	1.71E-08	1.35E-08
	2859	2851	8.69E+04	8.55E+04	8.66	10.14	1.15E+03	9.63E+02	2.78E-08	2.33E-08
sum:			2.62E+06	2.62E+06					8.03E-07	6.67E-07
avg:	1737	1743	5.23E+04	5.23E+04	5.69	7.63	9.64E+02	6.88E+02	1.61E-08	1.33E-08

TABLE 2Ø
Test results for 2ØØ keV neutrons producing protons within the gas cavity

	#Electrons		Energy Deposited (eV)		Tracklength (cm)		LET (Mev*cm2/g)		Dose Equiv (Sv)	
	MC	AL	MC	AL	MC	AL	MC	AL	MC	AL
	1509	1402	4.58E+04	4.21E+04	4.73	7.63	1.11E+03	6.30E+02	1.47E-08	9.08E-09
	1595	1593	4.89E+04	4.78E+04	5.58	6.02	1.00E+03	9.06E+02	1.57E-08	1.30E-08
	264	316	7.95E+03	9.48E+03	1.83	4.47	4.97E+02	2.42E+02	1.21E-09	
	1300	1298	3.96E+04	3.89E+04	3.79	5.16	1.19E+03	8.63E+02	1.27E-08	9.69E-09
	1717	1721	5.05E+04	5.16E+04	5.00	5.83	1.15E+03	1.01E+03	1.62E-08	1.65E-08
	699	701	2.12E+04	2.10E+04	2.25	3.35	1.07E+03	7.16E+02	6.77E-09	4.54E-09
	3003	3002	8.97E+04	9.01E+04	10.73	11.09	9.55E+02	9.27E+02	2.45E-08	2.46E-08
	144	287	4.36E+03	8.61E+03	0.49	3.69	1.01E+03	2.67E+02	1.40E-09	9.73E-10
	2811	2824	8.38E+04	8.47E+04	8.39	9.99	1.14E+03	9.69E+02	2.68E-08	2.31E-08
	3	41	3.20E+01	1.23E+03	0.00	1.41	0.00E+00	9.93E+01	5.85E-13	6.35E-11
	169	180	5.18E+03	5.40E+03	0.49	2.00	1.22E+03	3.08E+02	1.66E-09	6.11E-10
	920	879	2.73E+04	2.64E+04	2.81	6.63	1.11E+03	4.54E+02	8.74E-09	
	539	516	1.65E+04	1.55E+04	3.35	3.69	5.61E+02	4.79E+02	3.11E-09	2.35E-09
	485	453	1.40E+04	1.36E+04	1.41	4.74	1.14E+03	3.27E+02	4.49E-09	1.54E-09
	3223	3212	9.60E+04	9.64E+04	9.50	10.08	1.15E+03	1.09E+03	3.07E-08	3.09E-08
	1144	1123	3.42E+04	3.37E+04	3.54	4.51	1.10E+03	8.54E+02	1.10E-08	8.38E-09
	1662	1671	5.01E+04	5.01E+04	5.60	6.84	1.02E+03	8.37E+02	1.60E-08	1.25E-08
	3370	3355	1.01E+05	1.01E+05	10.46	11.00	1.10E+03	1.05E+03	3.22E-08	3.22E-08
	623	624	1.94E+04	1.87E+04	2.03	3.55	1.09E+03	6.02E+02	6.22E-09	3.53E-09
	2119	2119	6.34E+04	6.36E+04	6.05	7.13	1.20E+03	1.02E+03	2.03E-08	2.04E-08
	0	30	0.00E+00	9.00E+02	0.00	2.24	0.00E+00	4.60E+01	0.00E+00	2.47E-11
	376	380	1.14E+04	1.14E+04	1.11	2.12	1.18E+03	6.14E+02	3.66E-09	2.15E-09
	816	839	2.47E+04	2.52E+04	2.74	4.37	1.03E+03	6.58E+02	7.89E-09	5.43E-09
	2522	2526	7.54E+04	7.58E+04	7.52	8.53	1.15E+03	1.01E+03	2.41E-08	2.43E-08
	1850	1822	5.57E+04	5.47E+04	5.26	6.06	1.21E+03	1.03E+03	1.78E-08	1.75E-08
	144	155	4.42E+03	4.65E+03	0.83	2.60	6.07E+02	2.04E+02	8.33E-10	3.80E-10
	1414	1407	4.34E+04	4.22E+04	4.47	6.08	1.11E+03	7.93E+02	1.39E-08	1.05E-08
	3502	3506	1.05E+05	1.05E+05	10.72	11.00	1.12E+03	1.09E+03	3.37E-08	3.37E-08
	325	307	9.95E+03	9.21E+03	1.19	2.24	9.55E+02	4.70E+02	2.71E-09	1.40E-09
	226	251	6.87E+03	7.53E+03	0.75	3.00	1.04E+03	2.87E+02	2.20E-09	8.51E-10
sum:			1.16E+06	1.16E+06					3.61E-07	3.10E-07
avg:	1282	1285	3.85E+04	3.85E+04	4.09	5.57	9.74E+02	6.62E+02	1.20E-08	1.03E-08

TABLE 21
Test results for 200 keV neutrons producing carbon ions within the gas cavity

	#Electrons		Energy Deposited (eV)		Tracklength (cm)		LET (Mev*cm2/g)		Dose Equiv (Sv)	
	MC	AL	MC	AL	MC	AL	MC	AL	MC	AL
	480	392	2.16E+04	1.18E+04	0.53	3.35	4.68E+03	4.00E+02	7.92E-09	1.78E-09
	248	225	1.77E+04	6.75E+03	1.04	2.00	1.94E+03	3.85E+02	5.65E-09	1.02E-09
	9	0	1.33E+03	0.00E+00	0.21	0.00	7.14E+02	0.00E+00	2.88E-10	0.00E+00
	377	380	2.31E+04	1.14E+04	0.95	2.55	2.79E+03	5.11E+02	8.43E-09	2.15E-09
	375	374	2.48E+04	1.12E+04	1.17	2.52	2.43E+03	5.08E+02	9.08E-09	2.11E-09
	225	223	1.68E+04	6.69E+03	0.99	1.79	1.93E+03	4.27E+02	5.37E-09	1.01E-09
	783	715	4.19E+04	2.15E+04	1.62	3.00	2.95E+03	8.16E+02	1.53E-08	5.34E-09
	247	216	1.73E+04	6.48E+03	0.95	4.74	2.07E+03	1.56E+02	6.32E-09	5.30E-10
	888	681	4.77E+04	2.04E+04	1.68	3.16	3.25E+03	7.38E+02	1.75E-08	
	343	206	2.23E+04	6.18E+03	0.86	2.00	2.95E+03	3.53E+02	8.16E-09	9.36E-10
	351	349	2.23E+04	1.05E+04	1.05	2.41	2.42E+03	4.97E+02	8.15E-09	1.59E-09
	29	19	3.72E+03	5.70E+02	0.39	1.50	1.10E+03	4.34E+01	1.19E-09	1.56E-11
	725	717	4.09E+04	2.15E+04	1.54	3.89	3.03E+03	6.32E+02	1.50E-08	4.64E-09
	757	684	3.75E+04	2.05E+04	1.05	2.00	4.08E+03	1.17E+03	1.37E-08	6.57E-09
	69	64	6.05E+03	1.92E+03	0.51	0.76	1.35E+03	2.88E+02	1.94E-09	2.17E-10
	979	977	5.16E+04	4.90E+04	1.87	1.73	3.15E+03	3.23E+03	1.89E-08	1.79E-08
	903	886	4.86E+04	2.66E+04	1.77	3.87	3.14E+03	7.84E+02	1.78E-08	6.61E-09
	424	450	2.54E+04	1.35E+04	1.17	2.12	2.48E+03	7.27E+02	9.28E-09	2.91E-09
	1081	1078	5.56E+04	5.34E+04	1.87	1.82	3.39E+03	3.35E+03	2.03E-08	1.95E-08
	5	0	1.12E+03	0.00E+00	0.14	0.00	9.03E+02	0.00E+00	3.06E-10	0.00E+00
	1089	1083	5.49E+04	3.25E+04	1.86	3.50	3.37E+03	1.06E+03	2.01E-08	1.04E-08
	109	107	1.03E+04	3.21E+03	0.73	1.09	1.62E+03	3.36E+02	3.30E-09	3.63E-10
	47	29	4.60E+03	8.70E+02	0.34	1.00	1.55E+03	9.93E+01	1.47E-09	4.49E-11
	432	433	2.75E+04	1.30E+04	1.24	2.80	2.54E+03	5.31E+02	1.01E-08	2.45E-09
	74	73	7.22E+03	2.19E+03	0.58	1.50	1.41E+03	1.67E+02	2.31E-09	1.79E-10
	863	746	4.66E+04	2.24E+04	1.70	2.80	3.13E+03	9.14E+02	1.70E-08	6.10E-09
	171	173	1.41E+04	5.19E+03	0.83	2.12	1.94E+03	2.79E+02	4.50E-09	5.87E-10
	162	162	1.31E+04	4.86E+03	0.82	1.45	1.82E+03	3.83E+02	4.18E-09	7.36E-10
	98	37	8.41E+03	1.11E+03	0.46	1.00	2.11E+03	1.27E+02	3.08E-09	5.73E-11
	437	443	2.70E+04	1.33E+04	1.26	2.82	2.45E+03	5.37E+02	9.89E-09	2.50E-09
sum:			7.41E+05	3.98E+05					2.66E-07	9.83E-08
avg:	426	397	2.47E+04	1.33E+04	1.04	2.18	2.42E+03	6.48E+02	8.88E-09	3.28E-09

TABLE 22
Test results for 3Ø keV neutrons producing protons at the inner wall surface

	#Electrons		Energy Deposited (eV)		Tracklength (cm)		LET (Mev*cm2/g)		Dose Equiv (Sv)	
	MC	AL	MC	AL	MC	AL	MC	AL	MC	AL
	171	156	5.15E+03	4.68E+03	1.59	2.83	3.69E+02	1.89E+02	7.79E-10	3.83E-10
	0	0	0.00E+00	0.00E+00	0.00	0.00	0.00E+00	0.00E+00	0.00E+00	0.00E+00
	43	58	1.45E+03	1.74E+03	0.57	1.41	2.93E+02	1.41E+02	1.64E-10	8.98E-11
	278	193	8.27E+03	5.79E+03	1.94	2.12	4.87E+02	3.12E+02	1.25E-09	6.55E-10
	88	109	2.52E+03	3.27E+03	0.93	3.00	3.10E+02	1.25E+02	2.84E-10	1.69E-10
	0	0	0.00E+00	0.00E+00	0.00	0.00	0.00E+00	0.00E+00	0.00E+00	0.00E+00
	413	408	1.28E+04	1.22E+04	2.79	3.75	5.22E+02	3.73E+02	2.40E-09	1.85E-09
	310	320	9.61E+03	9.60E+03	2.31	3.50	4.75E+02	3.13E+02	1.46E-09	1.09E-09
	0	35	1.37E+02	1.05E+03	0.07	1.41	2.22E+02	8.48E+01	1.12E-11	5.42E-11
	2	39	1.77E+02	1.17E+03	0.09	2.12	2.35E+02	6.30E+01	1.45E-11	3.21E-11
	5	0	2.38E+02	0.00E+00	0.11	0.00	2.48E+02	0.00E+00	1.95E-11	0.00E+00
	71	86	2.06E+03	2.58E+03	0.57	1.00	4.09E+02	2.95E+02	3.11E-10	2.92E-10
	141	148	4.12E+03	4.44E+03	1.39	2.24	3.40E+02	2.27E+02	4.66E-10	3.63E-10
	150	167	4.37E+03	5.01E+03	1.36	3.35	3.68E+02	1.71E+02	6.61E-10	4.10E-10
	218	190	6.42E+03	5.70E+03	1.73	2.00	4.23E+02	3.25E+02	9.72E-10	6.44E-10
	350	354	1.03E+04	1.06E+04	2.22	2.12	5.30E+02	5.72E+02	1.94E-09	2.00E-09
	115	138	3.78E+03	4.14E+03	1.30	2.00	3.31E+02	2.36E+02	4.27E-10	3.39E-10
	202	216	5.92E+03	6.48E+03	1.55	2.00	4.35E+02	3.70E+02	8.96E-10	9.82E-10
	166	172	5.07E+03	5.16E+03	1.48	3.16	3.91E+02	1.86E+02	7.68E-10	4.22E-10
	411	394	1.29E+04	1.18E+04	2.58	4.24	5.74E+02	3.18E+02	2.44E-09	1.34E-09
	210	215	6.44E+03	6.45E+03	1.86	2.60	3.95E+02	2.84E+02	9.76E-10	7.29E-10
	361	356	1.06E+04	1.07E+04	2.29	3.35	5.29E+02	3.64E+02	2.00E-09	1.62E-09
	237	237	6.95E+03	7.11E+03	1.73	2.24	4.58E+02	3.63E+02	1.05E-09	1.08E-09
	0	0	0.00E+00	0.00E+00	0.00	0.00	0.00E+00	0.00E+00	0.00E+00	0.00E+00
	12	41	4.98E+02	1.23E+03	0.27	2.50	2.08E+02	5.62E+01	4.07E-11	3.38E-11
	166	158	4.93E+03	4.74E+03	1.36	2.60	4.14E+02	2.08E+02	7.47E-10	3.88E-10
	247	258	7.81E+03	7.74E+03	1.99	2.80	4.49E+02	3.16E+02	1.18E-09	8.75E-10
	389	395	1.23E+04	1.19E+04	2.67	3.75	5.26E+02	3.61E+02	2.31E-09	1.80E-09
	0	0	0.00E+00	0.00E+00	0.00	0.00	0.00E+00	0.00E+00	0.00E+00	0.00E+00
	90	86	2.90E+03	2.58E+03	0.73	1.00	4.53E+02	2.95E+02	4.40E-10	2.92E-10
sum:			1.48E+05	1.48E+05					2.40E-08	1.79E-08
avg:	162	164	4.92E+03	4.93E+03	1.25	2.10	3.46E+02	2.18E+02	8.01E-10	5.97E-10

TABLE 23
Test results for 3Ø keV neutrons producing protons within the gas cavity

	#Electrons		Energy Deposited (eV)		Tracklength (cm)		LET (Mev*cm2/g)		Dose Equiv (Sv)	
	MC	AL	MC	AL	MC	AL	MC	AL	MC	AL
	485	486	1.43E+04	1.46E+04	2.95	4.97	5.55E+02	3.35E+02	2.70E-09	1.65E-09
	648	641	1.93E+04	1.92E+04	2.69	3.06	8.17E+02	7.17E+02	4.80E-09	4.15E-09
	880	880	2.68E+04	2.64E+04	4.56	4.45	6.71E+02	6.78E+02	5.78E-09	5.70E-09
	772	720	2.38E+04	2.16E+04	3.36	6.55	8.08E+02	3.77E+02	5.92E-09	3.27E-09
	392	390	1.20E+04	1.17E+04	2.59	3.87	5.28E+02	3.45E+02	2.26E-09	1.32E-09
	311	307	9.36E+03	9.21E+03	2.22	3.06	4.82E+02	3.44E+02	1.42E-09	1.04E-09
	395	384	1.19E+04	1.15E+04	1.54	3.54	8.84E+02	3.72E+02	3.25E-09	1.75E-09
	351	332	1.05E+04	9.96E+03	2.43	3.35	4.91E+02	3.39E+02	1.58E-09	1.13E-09
	442	421	1.32E+04	1.26E+04	2.81	4.68	5.36E+02	3.08E+02	2.49E-09	1.43E-09
	519	516	1.58E+04	1.55E+04	3.14	3.13	5.75E+02	5.65E+02	2.98E-09	2.92E-09
	118	123	3.78E+03	3.69E+03	1.26	2.60	3.44E+02	1.62E+02	4.28E-10	3.02E-10
	276	259	8.56E+03	7.77E+03	1.16	2.60	8.45E+02	3.42E+02	2.13E-09	8.78E-10
	348	346	1.06E+04	1.04E+04	2.46	2.39	4.91E+02	4.96E+02	1.60E-09	1.57E-09
	312	311	9.52E+03	9.33E+03	2.24	3.67	4.86E+02	2.90E+02	1.44E-09	1.06E-09
	369	373	1.13E+04	1.12E+04	2.61	2.52	4.96E+02	5.08E+02	1.72E-09	2.11E-09
	314	316	9.19E+03	9.48E+03	2.12	2.83	4.96E+02	3.83E+02	1.39E-09	1.44E-09
	405	398	1.22E+04	1.19E+04	1.53	3.06	9.12E+02	4.45E+02	3.32E-09	1.81E-09
	405	412	1.20E+04	1.24E+04	2.67	3.54	5.13E+02	3.99E+02	2.26E-09	1.87E-09
	176	184	5.63E+03	5.52E+03	0.67	2.00	9.55E+02	3.15E+02	1.54E-09	6.24E-10
	407	362	1.24E+04	1.09E+04	1.65	2.50	8.57E+02	4.96E+02	3.09E-09	1.65E-09
	50	64	1.43E+03	1.92E+03	0.18	1.50	9.07E+02	1.46E+02	3.91E-10	9.90E-11
	492	498	1.51E+04	1.49E+04	2.64	3.05	6.54E+02	5.59E+02	3.26E-09	2.82E-09
	80	85	2.27E+03	2.55E+03	0.37	1.00	7.06E+02	2.91E+02	4.91E-10	2.88E-10
	48	48	1.57E+03	1.44E+03	0.68	0.62	2.65E+02	2.67E+02	1.78E-10	1.63E-10
	368	350	1.15E+04	1.05E+04	2.69	3.75	4.88E+02	3.20E+02	1.74E-09	1.19E-09
	717	721	2.14E+04	2.16E+04	3.73	3.90	6.55E+02	6.33E+02	4.61E-09	4.67E-09
	984	931	2.95E+04	2.94E+04	4.78	4.77	7.05E+02	7.04E+02	6.37E-09	6.35E-09
	253	258	7.94E+03	7.74E+03	2.10	1.97	4.32E+02	4.48E+02	1.20E-09	1.17E-09
	33	70	9.88E+02	2.10E+03	0.21	1.41	5.29E+02	1.70E+02	1.86E-10	1.72E-10
	532	532	1.67E+04	1.60E+04	2.72	3.19	7.00E+02	5.71E+02	3.60E-09	3.01E-09
sum:			3.60E+05	3.53E+05					7.41E-08	5.76E-08
avg:	396	392	1.20E+04	1.18E+04	2.23	3.12	6.26E+02	4.11E+02	2.47E-09	1.92E-09

TABLE 24
Test results for 3Ø keV neutrons producing carbon ions within the gas cavity

	#Electrons		Energy Deposited (eV)		Tracklength (cm)		LET (Mev*cm2/g)		Dose Equiv (Sv)	
	MC	AL	MC	AL	MC	AL	MC	AL	MC	AL
	75	78	8.24E+03	2.34E+03	0.61	0.88	1.55E+03	3.05E+02	2.64E-09	2.65E-10
	60	59	5.64E+03	1.77E+03	0.53	2.12	1.21E+03	9.53E+01	1.80E-09	9.13E-11
	87	76	8.33E+03	2.28E+03	0.61	2.24	1.56E+03	1.16E+02	2.67E-09	1.18E-10
	43	34	4.16E+03	1.02E+03	0.45	1.50	1.06E+03	7.77E+01	1.33E-09	5.26E-11
	58	62	6.57E+03	1.86E+03	0.54	0.74	1.39E+03	2.86E+02	2.10E-09	2.10E-10
	32	34	4.17E+03	1.02E+03	0.46	0.47	1.03E+03	2.46E+02	1.34E-09	8.34E-11
	0	0	4.00E+00	0.00E+00	.00	0.00	1.05E+02	0.00E+00	2.06E-13	0.00E+00
	70	70	7.51E+03	2.10E+03	0.60	0.81	1.43E+03	2.96E+02	2.41E-09	2.37E-10
	40	42	5.14E+03	1.26E+03	0.48	0.56	1.23E+03	2.58E+02	1.64E-09	1.42E-10
	24	0	3.23E+03	0.00E+00	0.39	0.00	9.48E+02	0.00E+00	8.80E-10	0.00E+00
	58	55	5.74E+03	1.65E+03	0.50	0.68	1.30E+03	2.77E+02	1.84E-09	1.87E-10
	69	60	6.55E+03	1.80E+03	0.57	1.00	1.31E+03	2.06E+02	2.10E-09	1.47E-10
	18	0	2.94E+03	0.00E+00	0.36	0.00	9.34E+02	0.00E+00	8.02E-10	0.00E+00
	13	0	2.64E+03	0.00E+00	0.31	0.00	9.60E+02	0.00E+00	7.19E-10	0.00E+00
	13	0	1.91E+03	0.00E+00	0.24	0.00	8.95E+02	0.00E+00	5.22E-10	0.00E+00
	60	62	6.89E+03	1.86E+03	0.56	0.74	1.40E+03	2.86E+02	2.21E-09	2.10E-10
	6	0	8.90E+02	0.00E+00	0.19	0.00	5.26E+02	0.00E+00	1.68E-10	0.00E+00
	18	0	3.00E+03	0.00E+00	0.36	0.00	9.42E+02	0.00E+00	8.19E-10	0.00E+00
	4	0	1.27E+03	0.00E+00	0.24	0.00	6.06E+02	0.00E+00	2.39E-10	0.00E+00
	81	84	7.38E+03	2.52E+03	0.55	0.92	1.54E+03	3.12E+02	2.36E-09	2.85E-10
	73	66	7.80E+03	1.98E+03	0.65	2.12	1.37E+03	1.07E+02	2.50E-09	1.02E-10
	10	0	2.31E+03	0.00E+00	0.28	0.00	9.31E+02	0.00E+00	6.30E-10	0.00E+00
	25	0	3.00E+03	0.00E+00	0.33	0.00	1.04E+03	0.00E+00	9.59E-10	0.00E+00
	43	49	5.56E+03	1.47E+03	0.49	0.63	1.29E+03	2.68E+02	1.78E-09	1.66E-10
	57	0	6.35E+03	0.00E+00	0.55	0.00	1.31E+03	0.00E+00	2.03E-09	0.00E+00
	9	0	1.54E+03	0.00E+00	0.25	0.00	7.04E+02	0.00E+00	3.32E-10	0.00E+00
	46	51	5.89E+03	1.53E+03	0.53	0.65	1.27E+03	2.71E+02	1.89E-09	1.73E-10
	4	0	9.79E+02	0.00E+00	0.18	0.00	6.10E+02	0.00E+00	1.85E-10	0.00E+00
	86	83	8.19E+03	2.49E+03	0.66	0.91	1.41E+03	3.11E+02	2.62E-09	2.82E-10
	14	0	2.01E+03	0.00E+00	0.30	0.00	7.67E+02	0.00E+00	5.01E-10	0.00E+00
sum:			1.36E+05	2.90E+04					4.20E-08	2.75E-09
avg:	40	32	4.53E+03	9.65E+02	0.43	0.57	1.09E+03	1.24E+02	1.40E-09	9.17E-11

REFERENCES

Br85 Brackenbush, L.W., McDonald, J.C., Endres, G.W.R., Quam, W., 1985, "Mixed Field Dose Equivalent Measuring Instruments," Radiation Protection Dosimetry, 10, 307-318.

Cr85 Cross, W.G., Ing, H., 1985, "Conversion and Quality Factors Relating Neutron Fluence and Dosimetric Quantities," Radiation Protection Dosimetry, 10, 29-42.

Gr85 Greening, J.R., 1985, Fundamentals of Radiation Dosimetry, Medical Physics Handbook 15, (Bristol, England: Adam Hilger Ltd).

ICRP71 International Commission on Radiological Protection, 1971, "Data for Protection against Ionizing Radiation from External Sources: Supplement to ICRP Publication 15," ICRP Publication 21, (Oxford: Pergamon Press).

ICRP77 International Commission on Radiological Protection, 1977, "Recommendations of the International Commission on Radiological Protection," ICRP Publication 26, (Oxford: Pergamon Press).

ICRU77 International Commission on Radiation Units and Measurements, 1977, "Neutron Dosimetry for Biology and Medicine," ICRU Report 26, (Washington, D.C.: ICRU Publications).

ICRU79 International Commission on Radiation Units and Measurements, 1979, "Average Energy Required to Produce an Ion Pair," ICRU Report 31, (Washington, D.C.: ICRU Publications).

In85 Ing, H., Piesch, E., 1985, "Status of Neutron Dosimetry," Radiation Protection Dosimetry, 10, 5-15.

Kn79 Knoll, G.F., 1979, Radiation Detection and Measurement, (New York: John Wiley & Sons).

NAS64 National Academy of Science / National Research Council, 1964, "Studies in Penetration of Charged Particles in Matter," Fano, U., editor, NAS/NRC Publication 1133, (Washington, D.C.: National Academy Press).

NCRP71 National Council on Radiation Protection and Measurements, 1971, "Protection Against Neutron Radiation," NCRP Report 38, (Washington, D.C.: NCRP Publications).

Ng85 Nguyen, V.D., Luccioni, C., Parmentier, N., 1985, "Average Quality Factor and Dose Equivalent Meter Based on Microdosimetry Techniques," Radiation Protection Dosimetry, 10, 277-282.

Pi85 Piesch, E., 1985, "Calibration Techniques for Personnel Dosemeters in Stray Neutron Fields," Radiation Protection Dosimetry, 10, 159-173.

Ro79 Rogers, D.W.O., 1979, "Why Not to Trust a Neutron Remmeter," Health Physics, 37, 73-742.

Si82 Sims, C.S., Swaja, R.E., 1982, "Personnel Dosimetry Intercomparison Studies at the Health Physics Research Reactor: A Summary (1974-1980)," Health Physics, 42, 3-18.

Si85 Sims, C.S., Dickson, H.W., 1985, "Neutron Dosimetry Intercomparison Studies," Radiation Protection Dosimetry, 10, 331-340.

To82 Todo, A.S., Turner, J.E., Hamm, R.N., Wright, H.A., Poston, J.W., and Chiles, M.M., 1982, "A Study of Cylindrical, Energy-Proportional Pulse-Height Detectors for Measuring Microdosimetric Quantities," Radiation Protection, Proceedings of the Eighth Symposium on Microdosimetry, Julich, West Germany, Sept. 27 - Oct. 1, 1982, p. 1107-1116, Booz, J., Avert, H.G., editors, Commission of the European Communities, Brussels.

Tu84 Turner, J.E., Hamm, R.N., Hurst, G.S., Wright, H.A., and Chiles, M.M., 1984, "Studies of a Digital Approach to Neutron Dosimetry and Microdosimetry," in: Proceedings of the Fifth Symposium of Neutron Dosimetry, Neuherberg, FRG, September 17-21, 1984, sponsored by the Commission of the European Communities.

Tu85a Turner, J.E., Hamm, R.N., Hurst, G.S., Wright, H.A., and Chiles, M.M., 1985, "Digital Characterization of Particle Tracks for Microdosimetry," in: Proceedings of the Ninth Symposium on Microdosimetry, Toulouse, France, May, 1985, sponsored by the Commission of the European Communities, reprinted: 1985, Radiation Protection Dosimetry, 13, 45-48.

Tu85b Turner, J.E., Wright, H.A., Hamm, R.N., 1985, "A Monte Carlo Primer for Health Physicists", Health Physics, 48, 717-733.

Tu86 Turner, J.E., 1986, Atoms, Radiation & Radiation Protection, (Oxford: Pergamon Press).

ORNL/TM-10168

INTERNAL DISTRIBUTION

1-15. Wesley E. Bolch
16. M. M. Chiles
17. R. N. Hamm
18. C. S. Sims
19. R. E. Swaja
20-24. J. E. Turner
25. H. A. Wright
26. Central Research Library
27. Document Reference Section
28-29. Laboratory Records Department
30. Laboratory Records Department-RC
31. ORNL Patent Office

EXTERNAL DISTRIBUTION

32. H. A. Bevis, Wein Hall, Univ. of Florida, Gainesville, FL 32611.
33. W. E. Bolch, Black Hall, Univ. of Florida, Gainesville, FL 32611.
34. J. Booz, Institut für Medizin, Kernforschungsanlage Julich GmbH, Jülich, FRG.
35. A. E. S. Green, Space Sciences Research Bldg., Univ. of Florida, Gainesville, FL 32611.
36. W. C. Huber, Black Hall, Univ. of Florida, Gainesville, FL 32611.
37. G. S. Hurst, Univ. of Tennessee, One Pellissippi Center, Box 22238, Knoxville, TN 37933-0238
38. A. M. Jacobs, Nuclear Sciences Center, Univ. of Florida, Gainesville, FL 32611.
39. A. M. Kellerer, Inst. für Med. Strahlenkunde, Univ. Würzburg, D-8700 Würzburg, Versbacher Landstr. 1, FRG.
40. W. M. Lowder, Environmental Measurements Laboratory, U.S. Dept. of Energy, 376 Hudson St., New York, NY 10014.
41. H. G. Paretzke, GSF-Institut für Strahlenschutz, D-8042 Neuherberg, FRG.
42. C. E. Roessler, Black Hall, Univ. of Florida, Gainesville, FL 32611.
43. H. H. Rossi, Radiological Research Laboratory, Columbia Univ., 630 W. 168th St., New York, NY 10032.
44. G.M.A.A. Sordi, Inst. de Pesquisas Energeticas e Nucleares (CPRD/ARP) Caixa Postal 11049, Pinheiros CEP 05508, Sao Paulo, Brazil.
45. A. S. Todo, Inst. de Pesquisas Energeticas e Nucleares (CPRD/ARP) Caixa Postal 11049, Pinheiros CEP 05508, Sao Paulo, Brazil.
46. C. R. Williamson, University Programs Division, Oak Ridge Associated Universities, P. O. Box 117, Oak Ridge, TN 37831-0117.
47. R. W. Wood, Office of Health and Environmental Research, U.S. Dept. of Energy, Washington, D.C. 20545.
48. Office of Assistant Manager for Energy Research and Development, DOE/ORO.
49-50. Technical Information Center, Oak Ridge, Tennessee 37831.